Inter-comparison of Several Soil Moisture Downscaling Methods over the Qinghai-Tibet Plateau, China

Yuquan Qu[1,2], Zhongli Zhu[1,*], Carsten Montzka[2], Linna Chai[1], Shaomin Liu[1], Yong Ge[3,4], Jin Liu[1], Zheng Lu[1], Xinlei He[1], Jie Zheng[1], Tian Han[4,5]

1. State Key Laboratory of Earth Surface Processes and Resource Ecology, Faculty of Geographical Science, Beijing Normal University, Beijing 100875, China
2. Forschungszentrum Jülich, Institute of Bio- and Geosciences: Agrosphere (IBG-3), 52428 Jülich, Germany
3. State Key Laboratory of Resources and Environmental Information Systems, Institute of Geographic Sciences and Natural Resources Research, Chinese Academy of Sciences, Beijing 100101, China
4. University of Chinese Academy of Sciences, Beijing 100049, China
5. Laboratory of Remote Sensing and Geospatial Science, Northwest Institute of Eco-Environment and Resources, Chinese Academy of Sciences, Lanzhou 730000, Gansu, China

***Corresponding author.**

E-mail address: zhuzl@bnu.edu.cn (Z. Zhu).

Key Words:

Soil moisture; Downscaling; Methods comparison; Qinghai-Tibet plateau

ABSTRACT

Microwave remote sensing is able to retrieve soil moisture (SM) at an adequate level of accuracy. However, these microwave remotely sensed SM products usually have a spatial resolution of tens of kilometers which cannot satisfy the requirements of high to medium scale applications such as agricultural irrigation and

local water resource management. Several SM downscaling methods have been proposed to solve this mismatch by downscaling the coarse-scale SM to fine-scale (several kilometers or hundreds of meters). Although studies have been conducted over different climatic zones and from different data sets with good results, there is still a lack of a comprehensive comparison and evaluation between them to guide the production of high-resolution and high-accuracy SM data. Therefore, in this study we compared several SM downscaling methods (from 0.25° to 0.01°) based on polynormal fitting, physical model, machine learning and geostatistics over the Qinghai-Tibet plateau with a range of climate conditions from the evaluation including four aspects, that is, comparison with the original microwave product, comparison with in situ measurements, inter-comparison based on three-cornered hat (TCH) method, and a spatial feasibility analysis. The comparison results show that the method based on a physical model, in this case the Disaggregation based on Physical And Theoretical scale Change (DisPATCh) method, has the highest ability on preserving the feature of original microwave SM product, while to some extent, this ability could be a disadvantage for improving the accuracy of the downscaling results. In addition, soil evaporation efficiency (SEE) alone is not sufficient to represent SM spatial patterns over complex land surface. Geostatistics based area-to-area regression Kriging (ATARK) introduces the highest uncertainty caused by the overcorrection during the residual interpolation process while this process can also improve correlation (R) and correct the bias as well as provide more feasible spatial patterns and details. Two machine learning methods, the random forest (RF) and Gaussian process regression (GPR) show high stability on all comparison results but provide smoother spatial patterns. The multivariate statistical regression (MSR) method performs worst due to the fact that its simple linear regression model could not meet the requirement of SM fitting on complicated land surface. Moreover, all five downscaling methods show a declining accuracy after downscaling, which may be caused by the spatial mismatch on fine-scale and a

tendency that downscaling results will usually provide more spatial details from downscaling predictors while they cannot capture the temporal changes of the microwave SM product well. In general, this phenomenon tends to be more significant over heterogeneous land surface.

1. Introduction

Soil moisture (SM) is a key state variable for its important role in water, energy and carbon cycles, although it accounts for a little part of the liquid water on earth only (Mohanty et al., 2017; Montzka et al., 2017; Wu and Dickinson, 2004). It controls the process of evaporation, infiltration and runoff, governs vegetation water uptake, meanwhile it can be used to predict agricultural outputs, forecast flood/drought or wildfire events, and analyze climate changes (Alizadeh and Nikoo, 2018; Burapapol and Nagasawa, 2016; Madadgar et al., 2017; Schaefer and Magi, 2019; Wanders et al., 2014).

Several microwave satellites have been launched to provide temporally continuous and spatially complete SM information with missions, such as the METOP-A/B Advanced Scatterometer (ASCAT) (Bartalis et al., 2007), the Advanced Microwave Scanning Radiometer for Earth Observing System (AMSR-E) (Brocca et al., 2011; Jackson et al., 2005), the Advance Microwave Scanning Radiometer 2 (AMSR2) (Parinussa et al., 2015), the Soil Moisture and Ocean Salinity (SMOS) (Kerr et al., 2010), and the Soil Moisture Active Passive (SMAP) (Entekhabi et al., 2010). While the spatial resolution of these SM products is mostly at the scale of tens of kilometers, which cannot meet the research and application requirements at small and medium scale. Land surface process models, crop growth models and water management applications, for example, need SM information at higher resolution, i.e. several kilometers or even hundreds of meters (Crow et al., 2000; Fang et al., 2018).

To fill this gap, many SM downscaling methods have been proposed to obtain fine scale SM

information from coarse scale microwave products (Merlin et al., 2016; Peng et al., 2017; Sabaghy et al., 2018). Most of these methods are based on SM predictors from the temperature/vegetation feature space (Merlin et al., 2016; Peng et al., 2015; Wang et al., 2016), polynomial fitting methods (Chauhan et al., 2003; Chen et al., 2019; Piles et al., 2016; Sánchez-Ruiz et al., 2014), model based downscaling methods (Ines et al., 2013; Montzka et al., 2018; Nasta et al., 2018), machine learning methods (Guevara and Vargas, 2019; Im et al., 2016; Long et al., 2019; Park et al., 2015; Srivastava et al., 2013), geostatistical method (Jin et al., 2018a; Kim et al., 2017; Song et al., 2019), data fusion methods (Das et al., 2014; Lorenz et al., 2018; Montzka et al., 2016; Narayan et al., 2006; Zhan et al., 2006), and data assimilation methods (Naz et al., 2020; Pellenq et al., 2003; Sahoo et al., 2013).

Although different downscaling methods have been proposed and achieved good results, each type of the downscaling method has its own advantages, drawbacks, applicable conditions and assumptions. In this context, Peng et al. (2017) and Sabaghy et al. (2018) proposed systematic reviews of SM downscaling methods. Yu et al. (2008) used six downscaling methods based on linear interpolation and geographic weighted regression to successfully downscale SM from 25 km to 1 km in North America. The comparison results show that the methods based on geographic weighted regression have better performance and are less affected by the mosaic effect than linear extrapolation methods. Using the data from the Soil Moisture Experiments 4 (SMEX04) in southern Arizona, Kim and Hogue (2012) compared the soil wetness based method with the Disaggregation based on Physical And Theoretical scale Change (DisPATCh) method proposed by Merlin et al. (2009), and the temperature/vegetation feature space based polynomial fitting method. Results show the fine scale SM from the first two downscaling methods have higher accuracy. Wu et al. (2017) applied three SMAP based active-passive downscaling methods (official baseline algorithm, optional algorithm, and a change detection algorithm) from the Soil Moisture Active

Passive Experiment (SMAPEx) in Australia, with average root mean square errors (RMSE) of 0.019 m^3/m^3, 0.021 m^3/m^3, 0.026 m^3/m^3 respectively. Liu et al. (2018a) compared four machine learning methods including classification and regression trees (CART), K-nearest neighbors (KNN), Bayesian, and random forests (RF) over Northeast China. Results show that RF performs the best, has high correlation with the original microwave product and the in situ data, followed by CART, KNN and Bayesian. Jin et al. (2018b) compared geographically weighted area-to-area regression kriging (GWATARK) with a quadratic regression model (QRM) and area-to-area regression kriging (ATARK) at the upper reaches of the Heihe river basin. Results show that GWATARK performs better than QRM and ATARK, with a 20% decrease of the root-mean-square error (RMSE) than original SM product. Zhao et al. (2018) compared the RF method with a polynomial fitting model for the Iberian Peninsula based on the Moderate-Resolution Imaging Spectro-radiometer (MODIS) and SMAP ascending/descending SM products. Results show that RF outperforms another method with an unbiased RMSE (ubRMSE) of 0.022 m^3/m^3. Kim et al. (2018) applied a support vector regression (SVR) method to downscale SM in southwestern South Korea and compared it with a polynomial fitting method, with RMSE of 0.07 m^3/m^3 and 0.09 m^3/m^3, correlation coefficient (R) of 0.68 and 0.62, respectively.

However, these studies are usually limited to the comparison of same or similar types of downscaling methods or from different weather and climate conditions, there is still a lack of applicability analysis as well as comprehensive and systematic evaluations of the SM downscaling methods over a specific area, to guide the generation of high-resolution and high-precision downscaled SM products. To solve this problem, Sabaghy et al. (2020) performed a relatively comprehensive comparison in Australia between radar-based, radiometer-based, optical-based, and oversampling-based downscaling methods, while these methods are usually limited by the lack of radar observations which can match up the existing radiometer observations

spatially and temporally (radar-based), or by the ability of medium-scale (9-10 km, radiometer-based and oversampling-based methods) downscaling results in satisfying the needs of fine-scale SM applications.

Qinghai-Tibet plateau (QTP) is the source of seven major rivers in Asia, therefore, is also called the "water tower of Asia". In addition, its high altitude makes it a hotspot to study global climate changes. As an important variable indicating the interaction between land surface and atmosphere, SM with high-resolution and high-precision over the QTP is badly needed. Therefore, in this study a more detailed downscaling methods comparison was conducted over this region with a wide range of climate, land cover, and altitude conditions. We evaluated more widely used SM downscaling methods, including physical model based method, polynomial fitting based method, machine learning based method and geostatistical based method. The methods were evaluated from four aspects, that is: (1) comparison of the downscaled with original SM; (2) comparison of the downscaled SM with in situ observations; (3) inter-comparison based on the three-cornered hat (Tavella and Premoli, 1994) method; and (4) comparison of the spatial feasibility based on spatial patterns and details.

2. Study Area and Data

2.1. Study Area

With an average elevation of above 4000 m and a size of about 2.5 million km^2, the Qinghai-Tibet plateau (QTP, 26.5°–40°N and 73°–105°E) is the highest and largest mountain plateau in the world. It is characterized by high-altitude permafrost and glaciers (Cheng and Wu, 2007), so that it acts as an important water reservoir in East Asia and is called "the third pole" and "water tower of Asia" (Yang et al., 2011).

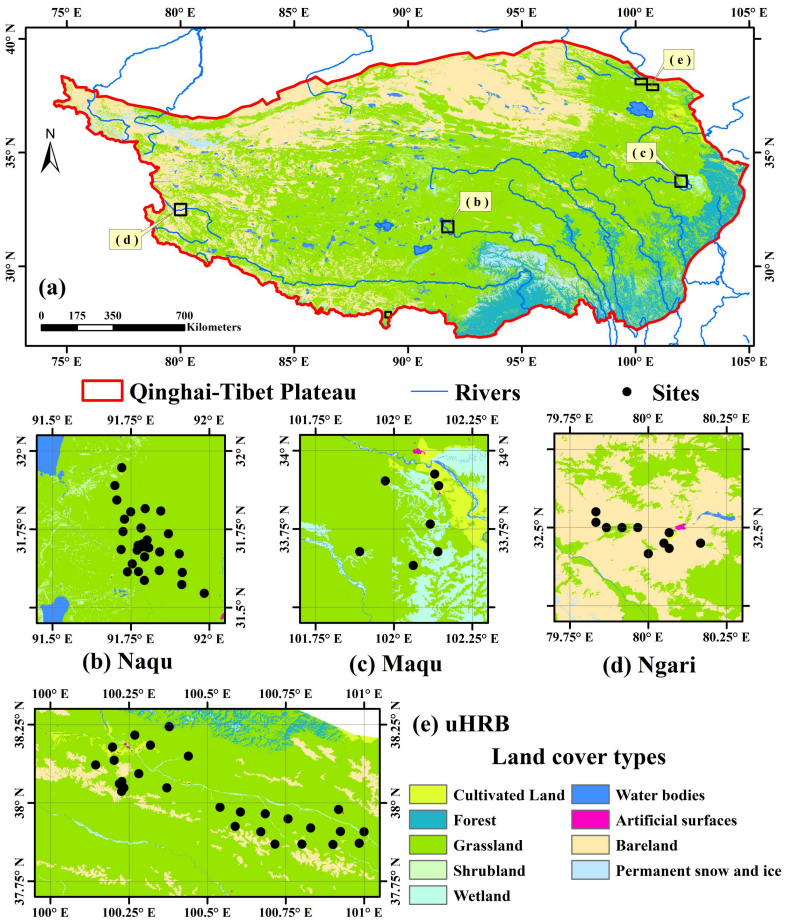

Fig.1. The study area (Qinghai-Tibet plateau) and the location as well as land cover of the in situ sites.

Most areas of the QTP are arid and semi-arid. In winter, controlled by Mongolian and Siberian highs, the climate of QTP is cold, arid and windy, while the climate is warm and wet in summer due to the Indian low (Ding et al., 2007). Precipitation mainly occurs from June to September, with relatively drier condition on winter and spring (Chen et al., 2013). As a major component of the global climate, water and energy cycles over the QTP play an important part in the Asian Monsoon (Zhang et al., 2003). The combination of high elevation with its special atmospheric, water and energy circulation, therefore, makes the QTP develop a series of "high-cold" vegetation types (Ni and Herzschuh, 2011). As shown in Fig. 1, the land cover distribution over the QTP follows a transitional gradient from the northwest to the southeast. The dry and cold climate resulted from high latitude and altitude on the northwestern QTP promotes barren land and

sparsely vegetated land cover. With increasing annual precipitation, the climate in the hinterland of the QTP changes to cold and wet, resulting in the development of high-cold meadow. Forests are found on the southeastern QTP, where the climate is warm and wet due to the lower altitude and latitude as well as the increase of precipitation.

2.2. Data Sets

2.2.1. Reconstructed Data

Several applications of soil moisture (SM) records require longer time series. For researches on the status and trends of SM over high mountainous areas, the SMAP data record (2015 to present) might not be sufficient, while the AMSR-E/AMSR2 mission, however, has a longer time series (from 2002 to present) but with lower accuracy than SMAP (Cui et al., 2017; Liu et al., 2019; Ray et al., 2017; Zeng et al., 2016). Qu et al. (2019) used the random forest method to train the SMAP SM product with AMSR-E/AMSR2 brightness temperature from five channels (H and V polarization of 10.7 GHz and 18.7 GHz, V polarization of 36.5 GHz) as well as auxiliary data (DEM, land cover, latitude, longitude, and day of the year) over the QTP, and rebuilt a Random Forest Soil Moisture (RFSM) product from 2002 to 2015 preserving the traits of SMAP well (R=0.95, RMSE=0.03 m^3/m^3) with high accuracy (R=0.75, RMSE=0.06 m^3/m^3, bias=-0.03 m^3/m^3) as compared to in situ measurements. Here, this reconstructed SM product (RFSM) from machine learning method was used for downscaling. The spatial resolution of RFSM is 0.25° according to the brightness temperature products from AMSR-E/AMSR2. As an example, the RFSM data of 2014 was used in this study to conduct the downscaling methods comparison to identify adequate methods for further generation of long-term high-resolution SM over the QTP.

To overcome the problem of the spatial/temporal discontinuity of the thermal infrared based land

surface temperature (LST) products over the QTP, a merged LST product (Zhang et al., 2019) from thermal infrared and microwave observations were used in this study. Space-borne thermal infrared (TIR) LST retrievals provide high spatial resolutions but suffer from cloud contaminations. By contrast, passive microwave (MW) LST products have all-weather capabilities but with a lower spatial resolution. To fill this gap, Zhang et al. (2019) integrated TIR and MW LST based on a temporal component decomposition method. The method decomposes LST into the components of annual temperature cycle (ATC), diurnal temperature cycle (DTC) prescribed by solar geometry, and weather temperature (WTC) driven by weather changes. The ATC is retrieved from clear-sky TIR LST and cloud-covered MW LST, respectively, and then combined by a temporal weighting method. The DTC is calculated from model-based LST product (CLDAS and GLDAS) by non-linear fitting, and the WTC is determined from subtracting ATC and DTC from the downscaled MW LST and then optimized by using a sliding window convolution strategy. The accuracy of this integrated TIR-MW LST product is 1.29–1.71 K, the spatial resolution is 1 km. In this study, the 1-km all-weather LST for the year 2014 was used and resampled to a resolution of 0.01° using a nearest neighbor resampling method.

2.2.2. Auxiliary Satellite Data

In order to feed the downscaling procedures, a range of auxiliary satellite data sets are required. The Global Land Surface Satellite (GLASS) is a high-precision, spatially continuous and long-term global product based on multi-source satellite sensors and ground-based measured data. Variables include leaf area index (LAI), surface broadband albedo (Albedo), fractional vegetation cover (FVC), gross primary production (GPP), evapotranspiration (ET), and broadband emissivity (BBE), etc. The GLASS products selected in this study are FVC (Jia et al., 2015), LAI (Xiao et al., 2014, 2016) and Albedo (Liu et al., 2013a,

2013b; Qu et al., 2014). The spatial resolution of the FVC product is 0.5 km, the spatial resolution of the LAI and Albedo product is 1 km, all these three products come with a sinusoidal projection and an 8-days temporal resolution. The data of 2014 was used in this study and all data can be downloaded from GLASS website (http://www.glass.umd.edu/Download.html).

Land cover data from Moderate-Resolution Imaging Spectro-radiometer (MODIS) was used in this study. The MCD12Q1 product includes six different classification schemes, we chose the International Geosphere-Biosphere Programme (IGBP) classification scheme with a spatial resolution of 0.5 km and a sinusoidal projection. The data of 2014 was used, and this product can be downloaded from the EARTHDATA website (https://search.earthdata.nasa.gov/).

Global 30 Arc-Second Elevation (GTOPO30) is a global digital elevation model (DEM) product developed by United States Geological Survey (USGS) with a resolution of 30-arc second (approximately 1 km), and an absolute accuracy of ±30 m. This DEM product can be downloaded from USGS website (http://eros.usgs.gov/#/Find Data/Products and Data Available/gtopo30 info). The precipitation data used in this study originates from CN05.1 (Wu and Gao, 2013), which is an interpolated 0.25° product based on more than 2000 station observations over China.

All auxiliary products such as GLASS (FVC, LAI and Albedo), MCD12Q1 and GTOPO30 were resampled to a longitude/latitude projection with a resolution of 0.01° using a nearest neighbor resampling method, to match the projection of microwave-based SM product whose resolution is 0.25°.

2.2.3. In Situ Soil Moisture Measurements

The in situ measurements used in this study were selected from four networks, namely the upper reach of Heihe River Basin (uHRB) (Li et al., 2013; Liu et al., 2018b), Naqu (Yang, 2013), Maqu and Ngari (Su

et al., 2011). Table 1 lists basic information about these four networks, more details can be found in Fig. 1 and the literature listed above. In this study, we assumed homogeneity of these 74 sites and that a single site value is representative for the mean value of a 0.01° pixel.

Standard deviations were calculated based on DEM to represent the heterogeneity of these four networks. Results show uHRB and Ngari (347.6 m and 380.9 m) have higher heterogeneity than Maqu and Naqu (151.6 m and 169.9 m).

Table 1. Information of 4 soil moisture in situ measurement networks.

Networks	uHRB	Maqu	Naqu	Ngari
Latitude	37.75°-38.5°N	33.5°-34.25°N	31°-32°N	79.75°-80.25°N
Longitude	100°-101.25°E	101.75°-102.75°E	91.6°-92.5°E	79.5°-79.75°E
Sampling interval	5 mins	15 mins	30 mins	15 mins
Depth used	4 cm	5 cm	5 cm	5 cm
Sites used	28	7	29	10
Time Period	04/2014-09/2014	04/2014-09/2014	04/2014-09/2014	04/2014-09/2014

3. Methodology

3.1. Spatial Soil Moisture Downscaling Predictor

SM downscaling predictors used in this study include LST, FVC, LAI, Albedo, soil evaporation efficiency (SEE), latitude, longitude and day or the year (DOY) from five aspects denoting energy, vegetation, dry/wet condition, geographic location and time information, respectively.

The SEE is defined as the actual to potential soil evaporation, can be retrieved from LST and FVC based on the method from Merlin et al. (2012). The calculation formula of SEE is as follow:

$$SEE = \frac{T_{s.max} - T_s}{T_{s.max} - T_{s.min}} \quad (1)$$

where $T_{s.max}$ and $T_{s.min}$ are the maximum and minimum value of the soil surface temperature over the study area, and T_s is the soil surface temperature at a given pixel, described as follow:

$$T_s = \frac{T - f_v \cdot T_v}{1 - f_v} \quad (2)$$

where T is the LST, f_v is FVC, and T_v is the vegetation temperature which can be calculated using the approach proposed by Moran et al. (1994). It should be noted that a correction for the elevation effects on T has been conducted based on the method proposed by Merlin et al. (2013):

$$T = T_{ori} + \gamma \cdot (H - \mathrm{H}_{LR}) \quad (3)$$

where T_{ori} is the original LST at a given pixel, γ is the mean lapse rate which is set to 0.006 ℃/m, H and H_{LR} are the altitude of a pixel (0.01°) and the mean altitude within the low resolution (0.25°) pixel, respectively.

3.2. Soil Moisture Downscaling Methods

Five downscaling methods were compared in this study, including a statistical regression based method, a physical model based method, two machine learning based methods, as well as a geostatistical based method.

3.2.1. Multivariate Statistical Regression

Multivariate statistical regression (MSR) refers to the establishment of a statistical relationship between SM and downscaling predictors under low resolution condition (microwave pixel scale), and then apply this statistical relationship to high resolution condition (target scale) by using high resolution downscaling predictors to obtain the downscaled SM at high resolution (Piles et al., 2016). The regression method used in this study is stepwise regression. The regression function can be described as follow:

$$SM = a_0 + \sum_{m=1}^{N} a_m \cdot A_m + \sum_{i.j=1}^{N} a_{ij} \cdot A_i \cdot A_j \ \ (i \geq j) \quad (4)$$

where a_0 is a constant, a_m and a_{ij} are regression coefficients, N is the number of the downscaling

predictors used, A_m, A_i and A_j are downscaling predictors.

3.2.2. DisPATCh

Disaggregation based on Physical And Theoretical scale Change (DisPATCh) is an updated version of the algorithms in Merlin et al. 2009, 2010, 2008. It aims at downscaling microwave SM from coarse to fine scale based on SEE given a semi-empirical model and a first order Taylor series expansion. The downscaling algorithm is shown as follow:

$$SM_{HR} = SM_{LR} + SM'(SEE_{LR}) \cdot (SEE_{HR} - SEE_{LR}) \quad (5)$$

where SM_{HR} is the downscaled SM at high resolution, SM_{LR} is the microwave SM at low resolution, $SM'(SEE_{LR})$ is the partial derivative of SM relative to SEE estimated at low resolution, SEE_{HR} and SEE_{LR} are SEE at high and low resolution respectively. The $SM'(SEE_{LR})$ can be calculated from daily SM and SEE observations. The function is described as follows (Malbéteau et al., 2016):

$$SM'(SEE_{LR}) = \frac{SM}{SEE} \quad (6)$$

Note that both EQ. (5) and EQ. (6) are linear functions, which ensures that the mean value of the downscaled SM at a microwave pixel is equal to the original microwave SM value.

3.2.3. Random Forest

The random forest (RF) approach as proposed by Breiman (2001) essentially belongs to a large branch of machine learning methods that uses ensembles. The basic idea is to integrate the results of different decision trees through ensemble learning.

The "random" denotes the randomization of data (rows) and variables (columns). First, row sampling is performed with a replacement sampling method. This makes sure the input samples of each tree are not the whole samples, which makes it relatively less prone to over-fitting. Then column sampling is performed

by randomly selecting a number of features m from the population M ($m < M$), and then select the best feature of m to completely split the samples. The "forest" denotes to the multiple independent decision trees. For an input sample, N trees will provide N decision results, and the RF will vote on all decision results, specifying the result with the most votes or choosing their average as the final output.

This method has many advantages without significantly increasing the processing time, i.e., it is insensitive to multivariate colinearity and default values, and has a certain anti-noise ability, and can handle high dimensional data (Ahmad et al., 2017).

3.2.4. Gaussian Process Regression

Gaussian process regression (GPR) is a non-parametric machine learning method that uses Gaussian Process (GP) prior distributions to perform the regression analysis. It is widely used in the fields of time series analysis, image processing and automation control (Hu and Wang, 2015; Li et al., 2015; Mihoub et al., 2016). It requires fewer parameters to be set than artificial neural networks, usually used for low dimensional and small sample regression problems where high accuracies are required.

The core theory of this algorithm uses the GP, which is a collection of multiple Gaussian distribution functions used to describe the distribution of data. Its nature is mainly described by the mean and covariance functions. Main assumption is that the prior distribution of variable y satisfies the following conditions:

$$y \sim N(\mu.K(x.x)) \quad (7)$$

where μ and $K(x.x)$ are the mean and covariance of y, respectively. The prior of joint probability distribution between observation variable y and predicted variable y^* can be described as:

$$\begin{bmatrix} y \\ y^* \end{bmatrix} \sim N\left\{ \begin{bmatrix} \mu \\ \mu^* \end{bmatrix}, \begin{bmatrix} K(x.x) & K(x.x^*) \\ K(x^*.x) & K(x^*.x^*) \end{bmatrix} \right\} \quad (8)$$

where μ and μ^* are mean value of y and y^*, x^* is new input variable samples, $K(x^*,x)=K(x,x^*)$ is covariance between x and x^*, $K(x,x)$ is covariance of x samples. GPR is able to use different kernel functions to represent the covariance during the training process, in this study, the square-exponential covariance kernel function was used.

After getting the prior distribution of y, and the joint probability distribution from EQ. (8), the posterior probability can be calculated based on Bayes´ formula. Therefore, the final estimation of $f(x^*)$ is performed by:

$$P(f(x^*)|f(x)) = \frac{P(f(x).f(x^*))}{P(f(x))} \quad (9)$$

where $P(f(x))$ is the prior distribution of y, $P(f.f(x^*))$ is the joint probability distribution, and $P(f(x^*)|f(x))$ is the posterior probability.

3.2.5. Area-to-Area Regression Kriging

The area-to-area regression Kriging (ATARK) (Jin et al., 2018b) downscaling process can be divided into two main parts: i) building the trend surface by MSR (EQ. (4)) and getting the residuals by removing trend surface from original microwave SM, and ii) performing area-to-area Kriging interpolation to the residuals and then add these fine resolution residuals to trend surface to finish the downscaling process. By this method, the residuals after regression can meet the second-order stationary condition and, therefore, modify the built trend surface.

After building the trend surface from MSR, the low-resolution regression residuals are constructed by subtracting the trend surface from the microwave SM values. Then the high-resolution residuals can be obtained from the nearby low-resolution residuals by:

$$\hat{r}(v_j) = \sum_{h=1}^{k} \lambda_{hj} \cdot r(v_h) \quad (10)$$

where $\hat{r}(v_j)$ is the residual to be estimated at a given fine scale pixel v_j, $r(v_h)$ is the neighboring residuals at coarse scale pixels, k is the number of the chosen neighboring coarse scale pixels, and λ_{hj} is the weight coefficient that can be calculated as follows:

$$\begin{cases} \sum_{i=1}^{k} \lambda_{ij} \cdot C(v_h.v_i) + \mu(o_j) = C(v_h.v_j). \forall\, h = 1.2.\cdots.k \\ \sum_{i=1}^{k} \lambda_{ij} = 1 \end{cases} \quad (11)$$

where $C(v_h.v_i)$ and $C(v_h.v_j)$ are area-to-area covariance, $\mu(o_j)$ is the Lagrange multiplier.

Finally, the resulting high-resolution residuals are added to the trend surface to obtain the downscaled SM.

3.3. Downscaling and Methods Comparison Procedure

Fig. 2 shows the downscaling procedure and comparison of the downscaling methods. Before the downscaling process, all the eight downscaling predictors were resampled to the resolution of 0.01° using a nearest neighbor resampling method. SEE, the downscaling predictor of DisPATCh is calculated from LST and FVC. The downscaling predictors of MSR and ATARK are LST, FVC, LAI, Albedo, SEE, longitude and latitude. As the models established by RF and GPR are with stronger simulation ability, apart from the downscaling predictors used in MSR and ATARK, the observation day of year (DOY) is added to ensure the stability of the downscaling relationship. It should be noted that the downscaling predictors used in MSR, ATARK, RF and GPR need to be normalized, and a denormalization process is performed after the high-resolution SM simulation to get the real downscaled SM.

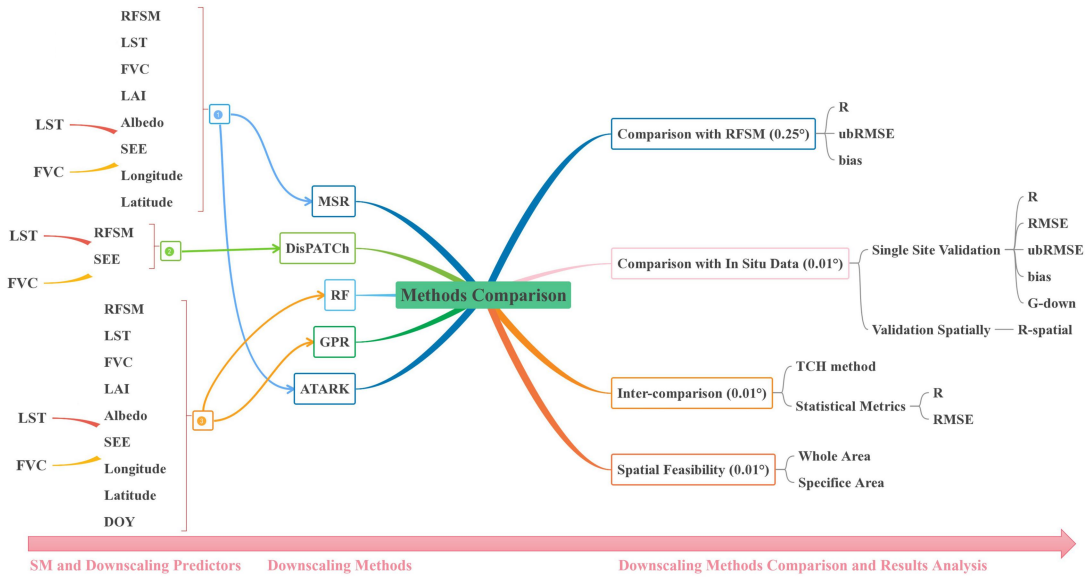

Fig.2. Flowchart of the soil moisture downscaling procedure and methods comparison.

After the downscaling procedure, the comparison was conducted based on four aspects, that is: (1) comparison with original microwave SM product, in this case is RFSM; (2) comparison of the downscaled SM with in situ observations based on single site and spatial correlation; (3) inter-comparison based on the three-cornered hat (TCH) method and statistical metrics; and (4) comparison of the spatial feasibility on the whole QTP and a specific area based on spatial patterns and details.

3.4. Statistical Metrics

The standard statistical metrics used in this study include correlation coefficient (R), root mean square error (RMSE), unbiased RMSE (ubRMSE), and bias, given by:

$$R = \frac{\sum_{i=1}^{N}(x_i - \bar{x})(y_i - \bar{y})}{\sqrt{\quad}} \quad (12)$$

$$RMSE = \sqrt{\frac{\sum_{i=1}^{N}(x_i - y_i)^2}{N}} \quad (13)$$

$$ubRMSE = \sqrt{\frac{\sum_{i-1}^{N}((x_i - \bar{x}) - (y_i - \bar{y}))^2}{N}} \quad (14)$$

$$bias = \frac{1}{N}\sum_{i=1}^{N}(x_i - y_i) \quad (15)$$

where $\bar{x}$ and $\bar{y}$ are mean value, x_i is the estimated value, y_i is the observed value, and N is the size of sample.

However, it is difficult to make a comprehensive quantitative comparison about the advantages and disadvantages of the downscaling method based on the verification results from a single evaluation metric. Therefore, this study used the G_{down} indicator (Merlin et al., 2015) to comprehensively evaluate the downscaling results from three aspects, that is efficiency gain (G_{effi}), precision gain (G_{prec}), and accuracy gain (G_{accu}), given by:

$$G_{down} = (G_{effi} + G_{prec} + G_{accu})/3 \quad (16)$$

$$G_{effi} = \frac{|1 - Slope_{LR}| - |1 - Slope_{HR}|}{|1 - Slope_{LR}| + |1 - Slope_{HR}|} \quad (17)$$

$$G_{prec} = \frac{|1 - R_{LR}| - |1 - R_{HR}|}{|1 - R_{LR}| + |1 - R_{HR}|} \quad (18)$$

$$G_{accu} = \frac{|bias_{LR}| - |bias_{HR}|}{|bias_{LR}| + |bias_{HR}|} \quad (19)$$

where, the subscript "LR" and "HR" indicate the statistical metrics on the microwave pixel scale and high-resolution scale respectively, and $Slope$ is the slope of microwave/downscaled SM against in situ data.

3.5. Three-Cornered Hat Method

As the quantity of in situ data is limited, a thorough performance analysis of downscaling methods within the whole QTP is a challenge. While the three-cornered hat (TCH) method (Tavella and Premoli, 1994) can estimate relative uncertainties among several products without prior information, independence between the tested products is not necessary if properly constrained. A time series can be split into true value and error by:

$$X_i = X_{true} + e_i. \forall i = 1.2.....N \quad (20)$$

where X_i is the i^{th} product time series, X_{true} is the true value, e_i is the error term and N is the total number of the product. The differences between the $N-1$ tested products X_i and a randomly selected reference product X_r are described as:

$$Y_{i.r} = X_i - X_r = e_i - e_r. \forall i = 1.2.....N-1 \quad (21)$$

where Y is a matrix with $N-1$ time series. If the covariance matrix of Y is $S = cov(Y)$, the $N \times N$ unknown covariance matrix of the individual noises R can be described as:

$$S = J \cdot R \cdot J^T \quad (22)$$

where $J = [I \ \ -U]$, I is a $(N-1) \times (N-1)$ identity matrix, U is a $(N-1)$ unit column vector.

To solve EQ. (22), Galindo and Palacio (1999) introduced a constrained minimization function based on Kuhn-Tucker theory, the objective function F can be obtained by:

$$F(R_{1N}.....R_{NN}) = \frac{1}{K^2} \cdot \sum_{i=1}^{N} \sum_{j=1}^{N} R_{ij}^2 . i < j \quad (23)$$

where $K = \sqrt[N-1]{|S|}$, R_{ij} is the elements of R. The constraint function G and the initial iteration conditions set as:

$$G(R_{1N}.....R_{NN}) = -\frac{|R|}{|S| \cdot K} < 0 \quad (24)$$

$$R_{iN}^0 = 0. i < N; R_{NN}^0 = \frac{1}{2 \cdot S^*} . S^* = U^T \cdot S^{-1} \cdot U \quad (25)$$

After obtaining the matrix R by minimizing EQ. (23), the square root of the diagonal values of R denotes the uncertainty of each product. The ratio of the uncertainty to the mean value of each product can be considered as relative uncertainty.

4. Results

4.1. Comparison of the Downscaled with Original Soil Moisture

To test the performance of the downscaling methods on preserving the traits of the original microwave SM product, the downscaling results at a resolution of 0.01° were averaged to 0.25°, then the statistical metrics (R, ubRMSE and bias) were calculated spatially, the results are shown in Fig. 3 and Fig. 4.

Fig. 3 shows that MSR, RF and GPR have worse performance on the northwest of the QTP, where the land cover is mainly barren or sparsely vegetated, according to the R value. ATARK has better performance over these areas originating from the residual correction process, but has worse performance at the border as well as south central of the QTP caused by the extensive topography. DisPATCh performs best among the five downscaling methods and the downscaling result is highly correlated with the original SM product over the whole QTP.

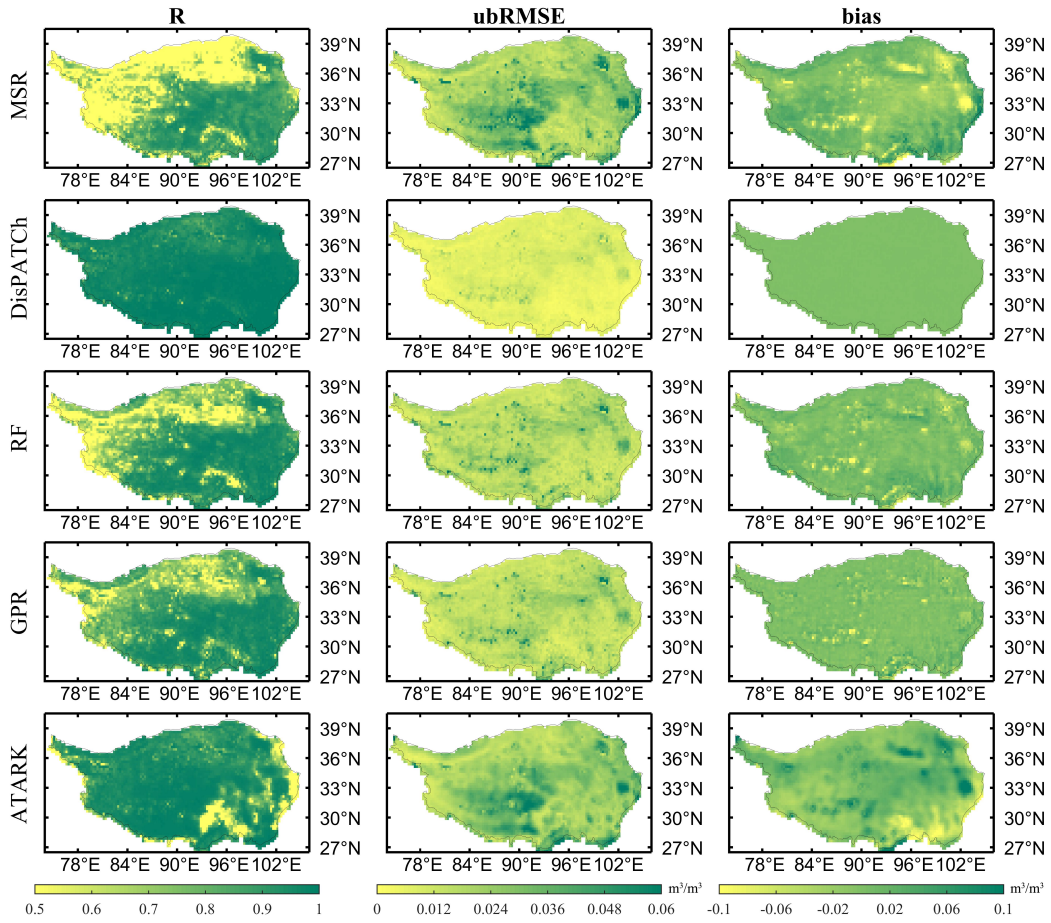

360

361 **Fig.3**. Spatial distribution of the comparison results (R, ubRMSE, bias) between the original microwave

362 product (RFSM) and the downscaling results.

363

364 As shown in the second column of Fig. 3, according to the ubRMSE value, RF and GPR show similar

365 spatial distribution, both of them have lower ubRMSE over the whole QTP. Both two statistical regression

366 methods (MSR and ATARK) also have similar spatial distribution with higher ubRMSE than RF and GPR,

367 but ATARK has smoother spatial pattern than MSR. Again, DisPATCh has the lowest ubRMSE value over

368 the whole QTP, also performs the best among the five methods.

369 The third column of Fig. 3 shows the spatial distribution of the bias. Results indicate that the bias of

370 DisPATCh is almost zero over the whole QTP, meaning the DisPATCh is the only unbiased downscaling

371 method in this study. GPR has better performance than RF, especially on the south and southwest of QTP.

The bias distribution of MSR and ATARK is opposite, and around water bodies MSR tends to underestimate and ATARK tends to overestimate.

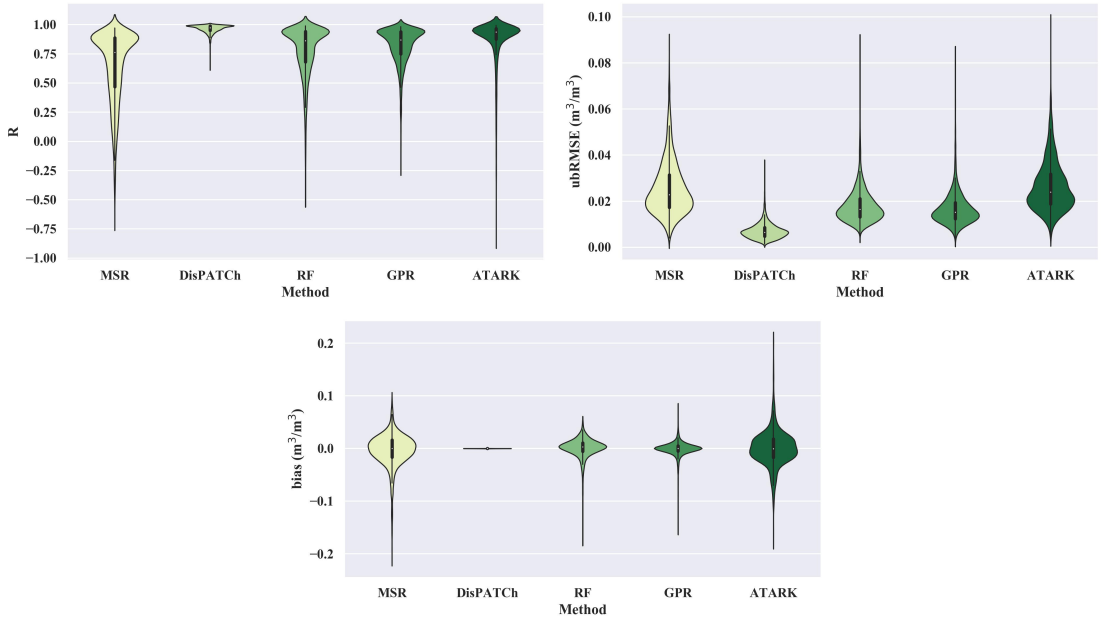

Fig.4. Violin plots (the black bar shows the third quartile, median and first quartile from top to bottom) of the value distribution of statistic metrics (R, ubRMSE, bias) between the original microwave product (RFSM) and the downscaling results.

Fig. 4 shows the value domain of these statistical metrics over the whole QTP. According to the R value, DisPATCh performs the best followed by ATARK, GPR, RF and MSR. From the ubRMSE, DisPATCh also performs the best followed by GPR, RF, MSR and ATARK. From the bias, DisPATCh almost has zero bias value followed by GPR, RF, MSR and ATARK, which is consistent with the results of ubRMSE.

4.2. Comparison of Downscaled and In Situ Soil Moisture

To evaluate the performance of the downscaling methods, the downscaling results were compared with

386 the in situ SM data at the 0.01° scale at four stations (totally 74 sites) during the unfrozen season (from
387 April 1st to September 30th). In addition, the validation of the RFSM against in situ SM observations is
388 performed at the 0.25° scale at all 74 sites. The verification results are shown in Appendix. 1 and Appendix.
389 2, where R, RMSE, ubRMSE, bias and G_{DOWN} are calculated separately.

390 Fig. 5 and Table 2 show the violin plots as well as the mean value of the of the validation results over
391 the all 74 sites. The distribution of the correlation coefficient of ATARK is most similar to RFSM, with
392 very close mean value, first and third quartile, and median (0.555 m^3/m^3 to 0.546 m^3/m^3) which means the
393 ATARK method can capture the temporal variation of the RFSM well, followed by DisPATCh, RF, GPR
394 and MSR (0.479 m^3/m^3, 0.472 m^3/m^3, 0.469 m^3/m^3 and 0.445 m^3/m^3, respectively).

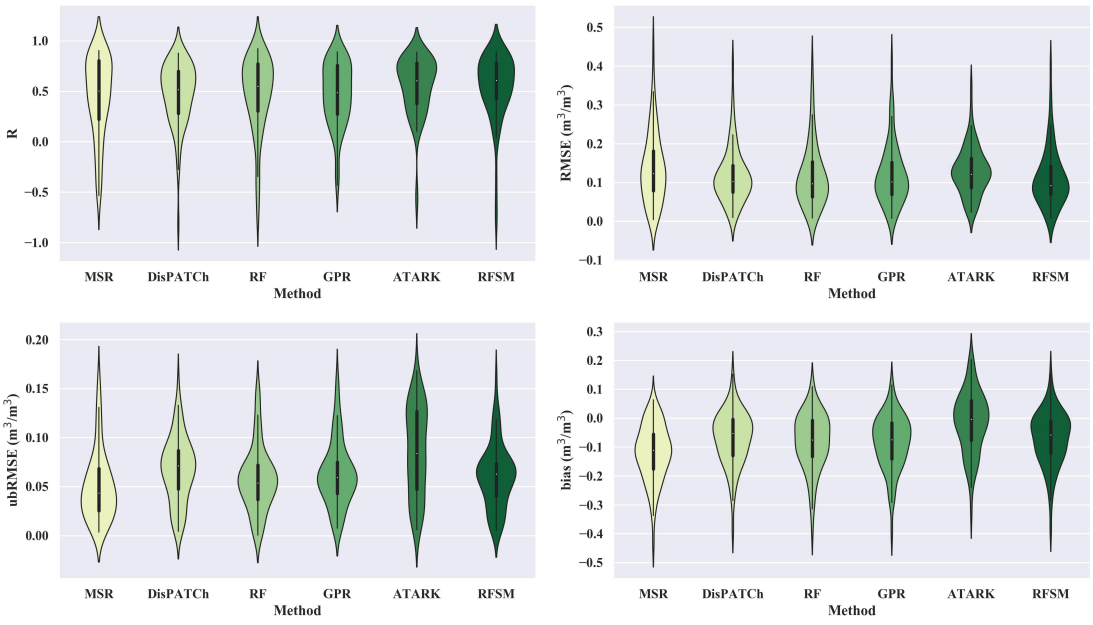

395

396 **Fig.5**. Violin plots (the black bar shows the third quartile, median and first quartile from top to bottom) of
397 the value distribution of statistic results (R, RMSE, ubRMSE, bias) between the downscaling results and in
398 situ soil moisture measurements.

399

400 For the RMSE value, the distribution patterns of DisPATCh, RF and GPR are more similar to RFSM

with most of the RMSE located near 0.1 m^3/m^3, while as shown in Table 2, DisPATCh and RF has lower mean value than GPR (0.118 m^3/m^3, 0.117 m^3/m^3 and 0.121 m^3/m^3 respectively), followed by ATARK and MSR (0.129 m^3/m^3 and 0.137 m^3/m^3). Meanwhile the MSR has a wider value range, which means it has lower stability over different sites according to RMSE. Note that all these five downscaling results lead to an increase of the RMSE compared to RFSM whose mean value is 0.112 m^3/m^3.

Based on ubRMSE, MSR performs best (0.051 m^3/m^3), followed by RF, GPR, DisPATCh and ATARK (0.058 m^3/m^3, 0.063 m^3/m^3, 0.068 m^3/m^3, 0.086 m^3/m^3 respectively). Based on the bias evaluation, the ranking is ATARK, DisPATCh, RF, GPR and MSR (-0.014 m^3/m^3, -0.069 m^3/m^3, -0.081 m^3/m^3, -0.083 m^3/m^3 and -0.119 m^3/m^3 respectively). As an unbiased downscaling method, DisPATCh has the closest bias value with its origin RFSM. MSR usually has a narrow violin indicating that this method is unstable when applied to different areas.

Note that these conclusions do not directly support the comparison results between the RFSM and downscaled SM as shown in Fig. 3 and Fig. 4, meaning that to some extent the ability of transferring the accuracy of the original microwave SM product could be a disadvantage for improving the accuracy of the downscaling results. For example, the MSR although has worse performance regarding ubRMSE when compared with RFSM, it has the best performance when compared with in situ observed SM, and DisPATCh performs better than ATARK on R when compared with RFSM, while ATARK has the highest R value when compared with in situ observed SM, even better than RFSM.

When comparing at different networks, MSR has worse R performance at uHRB, Maqu and Ngari, while at Naqu where the land cover is homogeneous grassland as shown in Fig. 1, MSR shows highest R. It also shows low ubRMSE and high bias at all four networks. ARARK has highest R at all four networks indicating the residual processing strategy is useful for capturing a higher portion of SM temporal changes

information, but usually introduce larger bias and fluctuation. RF and GPR have lower RMSE and ubRMSE at Naqu, but RF performs better than GPR at all four networks based on RMSE and ubRMSE as well as lowest RMSE at Naqu and Ngari.

Table 2. The mean value of the statistical results of the downscaled soil moisture against in situ measurements. The greener the color scheme, the better the statistical result. The color scheme is separately used to facilitate the comparison in each network.

In situ networks	Methods	Unfrozen season mean value					In situ networks	Methods	Unfrozen season mean value				
		R	RMSE	ubRMSE	bias	+ Gdown			R	RMSE	ubRMSE	bias	+ Gdown
uHRB (28 sites)	MSR	0.327	0.182	0.070	-0.159	25.0%	Maqu (7 sites)	MSR	0.249	0.144	0.076	-0.120	0.0%
	DisPATCh	0.390	0.150	0.070	-0.114	32.1%		DisPATCh	0.430	0.090	0.078	-0.032	28.6%
	RF	0.298	0.164	0.073	-0.127	28.6%		RF	0.323	0.094	0.079	-0.040	14.3%
	GPR	0.324	0.165	0.076	-0.126	35.7%		GPR	0.448	0.098	0.080	-0.038	42.9%
	ATARK	0.424	0.134	0.071	-0.073	50.0%		ATARK	0.469	0.129	0.091	0.088	28.6%
	RFSM	0.460	0.148	0.067	-0.114	-		RFSM	0.494	0.089	0.073	-0.035	-
Naqu (29 sites)	MSR	0.754	0.124	0.039	-0.111	37.9%	Ngari (10 sites)	MSR	0.013	0.046	0.014	-0.027	30.0%
	DisPATCh	0.659	0.113	0.080	-0.041	34.5%		DisPATCh	0.243	0.060	0.018	-0.053	30.0%
	RF	0.712	0.103	0.055	-0.064	58.6%		RF	0.371	0.045	0.012	-0.030	50.0%
	GPR	0.705	0.105	0.061	-0.063	58.6%		GPR	0.206	0.061	0.020	-0.054	20.0%
	ATARK	0.715	0.145	0.121	0.035	41.4%		ATARK	0.522	0.071	0.022	-0.063	50.0%
	RFSM	0.725	0.104	0.068	-0.045	-		RFSM	0.307	0.051	0.016	-0.042	-
All (74 sites)	MSR	0.445	0.137	0.051	-0.119	28.4%							
	DisPATCh	0.479	0.118	0.068	-0.069	32.4%							
	RF	0.472	0.117	0.058	-0.081	41.9%							
	GPR	0.469	0.121	0.063	-0.083	43.2%							
	ATARK	0.555	0.129	0.086	-0.014	44.6%							
	RFSM	0.546	0.112	0.061	-0.070	-							

According to G_{DOWN} shown in Table. 2, from the view of all four networks, there are only 28.4%, 32.4%, 41.9%, 43.2% and 44.6% of the sites with positive G_{DOWN} values for MSR, DisPATCh, RF, GPR and ATARK, respectively. This implies a negative effect of the downscaling process to the SM accuracy. This phenomenon is more obvious over heterogeneous land surface like uHRB and Maqu. At Naqu,

however, RF and GPR show more than 50 percent of positive G_{DOWN}. MSR, DisPATCh and ATARK also show higher proportion of positive values indicating that downscaling over homogeneous land surface could be more likely to keep the accuracy of RFSM or even improve the accuracy.

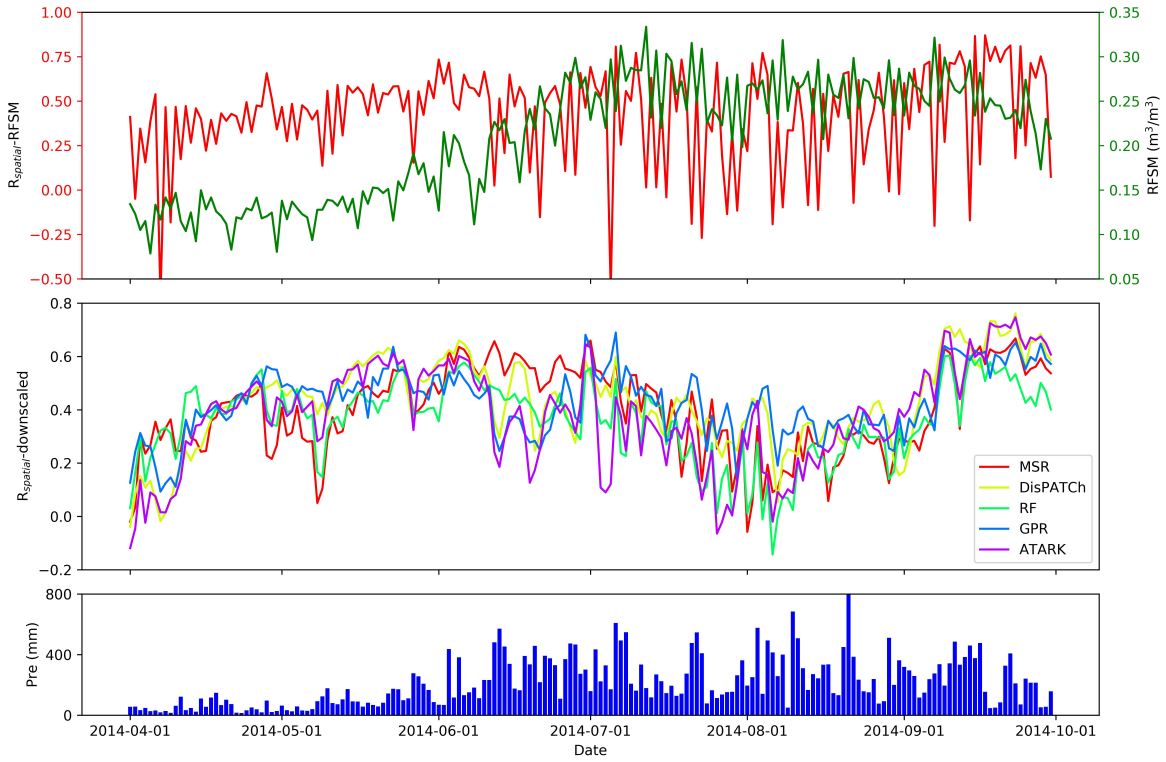

Fig.6. Spatial correlation ($R_{spatial}$) of original microwave product (RFSM) and the downscaled results with all 74 in situ sites over unfrozen season of 2014, as well as the average value of corresponding RFSM and precipitation.

To further test the temporal stability of the downscaling methods, the temporal course of the spatial correlation $R_{spatial}$ is plotted in Fig. 6. The results show that $R_{spatial}$ of RFSM changes dramatically during the seasons with precipitation. In April, when the QTP soils not evenly unfreeze and ponding water might cover the soil, the spatial surface SM cannot be captured adequately. Then $R_{spatial}$ increases until summer and the spatial patterns are adequately represented. Later in summer and autumn, SM variability decreases

with the increase of SM thus resulting in the decline of $R_{spatial}$. The large noise of $R_{spatial}$ could be resulted from the possibility that topography variations, land cover changes and precipitation cannot be detected in a 0.25° microwave pixel but could be detected by some in situ sites. While this seasonal trend is more obvious in the SM downscaling results. When the whole QTP is dry or wet, the low SM variability leads to lower spatial correlations between downscaled SM and in situ stations. The spatial correlation is highest during moderate SM conditions with highest SM variability (Zhao et al., 2013). An extensive precipitation event in summer and autumn reduces the spatial correlation $R_{spatial}$.

4.3. Inter-Comparison of Downscaling results

Considering that the direct comparison is limited by the quality and quantity of the in situ SM measurement, it is difficult to indicate the overall performance of the downscaling methods over the entire QTP. Therefore, the three-cornered hat (TCH) method was used in this study to compare the spatial distribution of the uncertainty between the five downscaling methods. In addition, an inter-comparison between the downscaling results is also performed by calculating R and RMSE between each two methods, the results are shown in Fig. 7 and Fig. 8.

It can be seen from Fig. 7 that the high uncertainty of DisPATCh is mainly concentrated on the boundary of microwave pixels with strong SM variability and around high SM areas. In addition, high uncertainty also appears close to water bodies where higher SM values appear as well as forest land cover in the southern part of the QTP. Both RF and GPR have high uncertainty in the Eastern part and around the Qinghai Lake in the Northeast of the QTP. GPR has higher uncertainty than RF in the forested southern part of the QTP. MSR and ATARK, both based on statistical regression, have similar uncertainty spatial distribution. Both results show higher uncertainty over high SM area around water bodies and wetlands in

the Eastern part and hinterland of the QTP. Generally, ATARK exhibits higher uncertainty than MSR especially on the Northeastern QTP and the grassland in the central part as well as forest in the South of the QTP. Fig. 7 also shows the spatial distribution of the downscaling results with minimum uncertainty, where GPR performs best in 33.2% of the QTP area, followed by RF 29.5%, DisPATCh 28.4%, MSR 8.1% and ATARK 0.8%.

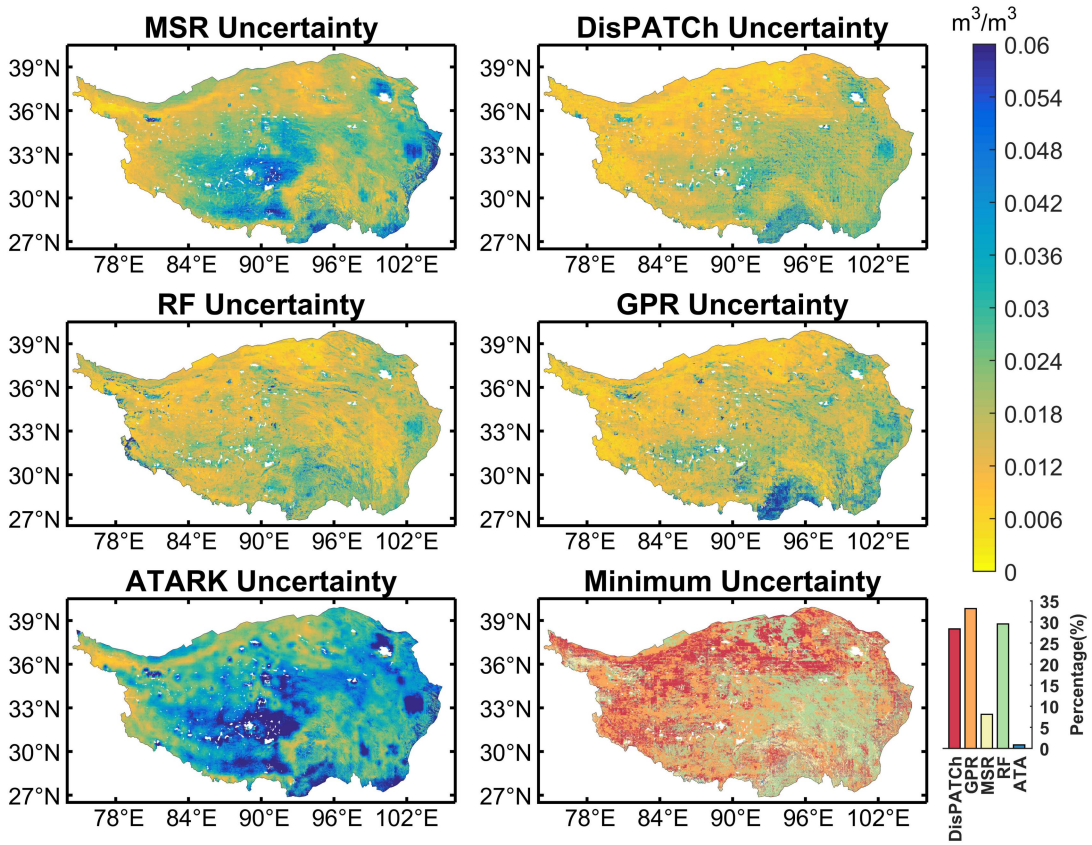

Fig.7. The three-cornered hat (TCH) comparison results between the five downscaled soil moisture and the spatial pattern where each downscaling method has minimum uncertainty among the five methods.

Fig. 8 presents the inter-comparison between each two methods. Results show that DisPATCh, RF and GPR have high correlation, with higher R values (from 0.81 to 0.85) and lower RMSE values (lower than 0.04 m^3/m^3); MSR performs worse with R lower than 0.8 (0.66, 0.73 and 0.51) and RMSE higher than 0.04 m^3/m^3 (0.049 m^3/m^3, 0.042 m^3/m^3, 0.081 m^3/m^3) against DisPATCh, GPR and ATARK; while although has

similar R values as MSR, ATARK performs worst with the highest RMSE (higher than 0.05 m^3/m^3) as compared to other methods.

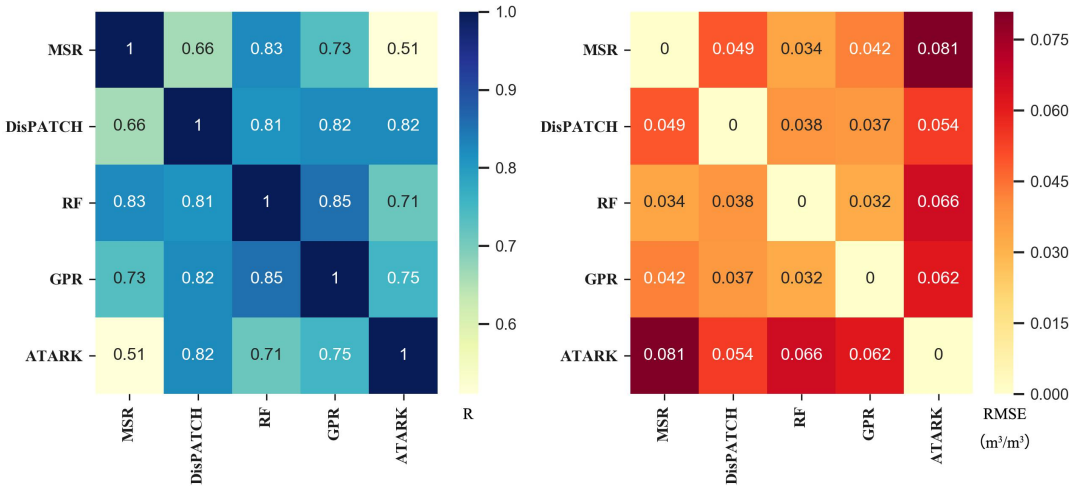

Fig.8. Inter-comparison between each two methods based on R and RMSE, as a supplement to the three-cornered hat (TCH) comparison results.

Note that the correlation between MSR and ATARK is the lowest even though they all based on polynomial-fitting and used the same downscaling predictors. The reason could be attributed to the residual interpolation process of ATARK. Compared to RF and GPR, although DisPATCh is downscaled from SEE, while RF and GPR are downscaled from LST, FVC, LAI, Albedo, SEE, longitude/latitude and DOY, they still have high correlation. This might be caused by the fact that DisPATCh have high ability on preserving the accuracy and spatial pattern of RFSM and machine learning methods have strong simulation ability. Another reason could be attributed to the high representativeness of LST to SM (Long et al., 2019), but this should be considered carefully. As the ability of MSR to capture the high dynamics of SM over the QTP is limited by its linear model, this fitting performance difference would induce the weaker correlation between MSR and RF/GPR. ATARK exhibits a higher bias than other methods when compared with RFSM (Fig. 3), therefore, in this inter-comparison it performs worst.

This phenomenon is similar to the direct comparison results against in situ data in Table 2, where DisPATCh, RF and GPR have similar performance and MSR performs worst while ATARK performs best regarding R and bias. This is also consistent with the results shown in Fig. 7 based on TCH method, that is, DisPATCh, RF and GPR have similar uncertainty, MSR has high uncertainty in some specific areas, and ATARK has the highest uncertainty over most area of the QTP.

4.4. Spatial Feasibility of the Downscaled Soil Moisture

In order to analyze the feasibility of the spatial distribution of the downscaling results, Fig. 9 and Fig. 10 compare the downscaling results with RFSM over the whole QTP and a specific area on the unfrozen season.

As shown in Fig. 9, all five methods can capture the temporal changes of RFSM, and DisPATCh, GPR as well as RF are consistently better capturing the spatial patterns of RFSM over the whole QTP. Considering that DisPATCh is an unbiased downscaling method, its ability to restore the spatial pattern of the original microwave product is the strongest, but because of the pixel-by-pixel downscaling process, despite a sliding window method is used, the mosaic effect is still relatively serious as shown in Fig. 9. While RF, to a certain extent, has a stronger smoothing effect than DisPATCh on the spatial trend. Due to the downscaling predictors used in this study contain latitude/longitude information which are at a low resolution and the fact that RF cannot predict values out of range of training sets, therefore, the new inputted fine scale latitude/longitude information would probably lead the predicted SM to nearest pixels SM values in the training sets at a coarse scale and induces the mosaic effect of downscaling results. But this phenomenon mainly occurs in areas with strong SM gradients, so that there is basically no mosaic phenomenon in areas with stable SM.

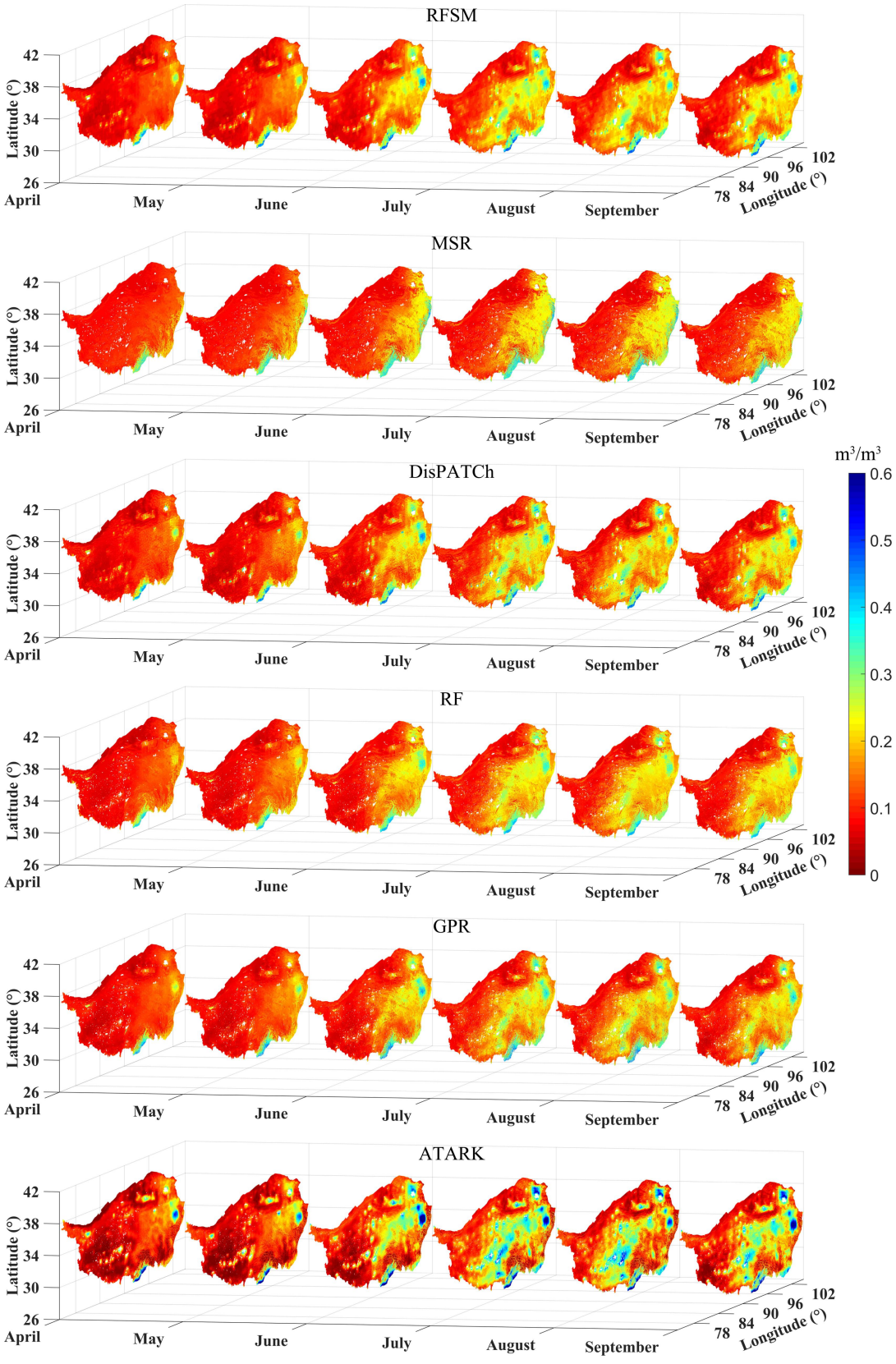

520

521 **Fig.9**. The spatial distribution of RFSM and five downscaling results over the unfrozen season of 2014.

522

Compared with RF, the spatial distribution of GPR is less affected by mosaic effect in some SM variable areas and is not as smooth as RF in SM stable areas, but on the whole there is a high degree of consistency with RF. MSR has a good response in the forest area only in the Southeastern QTP. But in other regions of QTP, its downscaling results lose the spatial details of SM, that is, the spatial distribution is too smooth, especially in areas with large gradients of SM. In contrast, ATARK underestimates SM in dry areas and overestimates SM in wet areas, which strengthens the spatial comparison of SM and highlights the SM spatial characteristics of QTP. This is because during the residual interpolation process, the residual of the high-resolution target pixels is affected by the surrounding high absolute value residuals, thus overestimating the residuals, and after these overestimated residuals are added to the regression trend surface, the overcorrecting phenomenon appears.

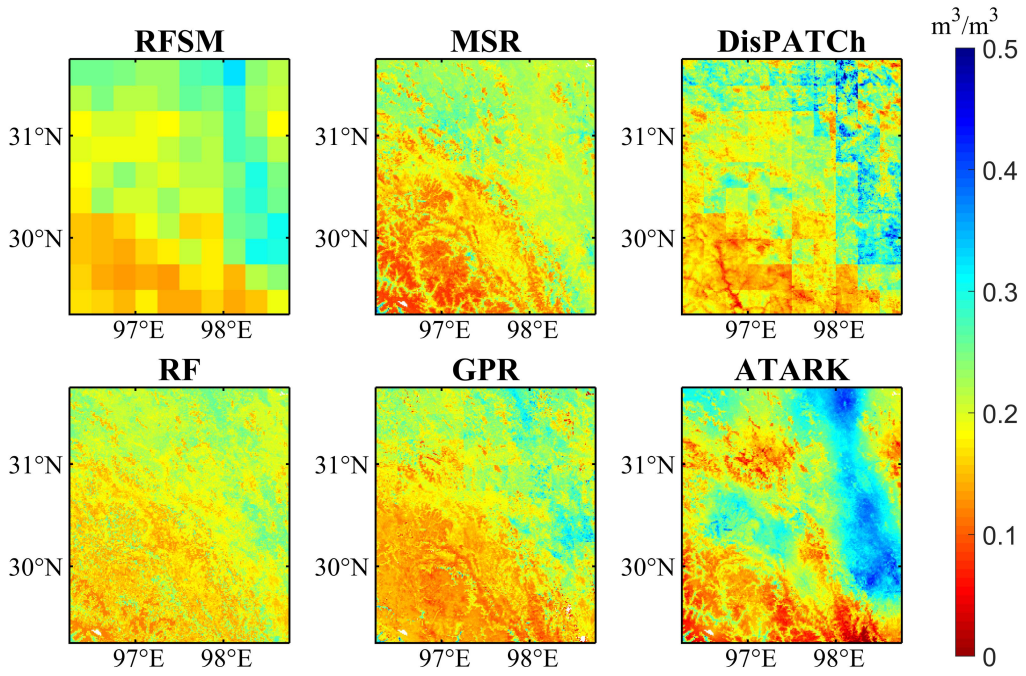

Fig.10. The spatial distribution of RFSM and five downscaling results within a specific area (29.25°-31.75°N, 96.25°-98.75°E) on July 1, 2014.

Fig. 10 shows spatial details of the downscaling results over a specific area. All results except MSR can keep the spatial pattern of RFSM well. While in the southwestern river valley, DisPATCh shows lower SM which indicates the possibly wrong SEE spatial pattern in this area, and that one downscaling predictor alone is not sufficient to represent spatial pattern and details on complex land surface. ATARK performs better by both providing spatial pattern from RFSM and spatial details from downscaling predictors than DisPATCh. MSR although can provide spatial details around the river valley, it weakens the spatial pattern of RFSM. Comparing with RF whose spatial pattern is smooth, GPR can provide more spatial details both in southwestern low SM areas and northeastern high SM areas.

5. Discussion

5.1. Downscaling Algorithms and Scale Effects

Based on the performance of the five downscaling results on preserving the traits of the original microwave product in Section 4.1, the reasonable order of performance is DisPATCh, GPR, RF, ATARK and MSR. This result is related to the scale effect introduced from their downscaling algorithm.

Scaling of environmental states and processes is a key issue in remote sensing research, and scale effects need to be considered in remote sensing analyses. The scale effects in this downscaling process mainly originate from two topics: (1) when the downscaling predictors were aggregated to low resolution, the scale effect caused by the nonlinearity on the retrieval process of the downscaling predictors. This kind of scale effect exists in all five downscaling methods, so that we decide to omit a thorough analysis. (2) The scale effect of the model, that is, whether the downscaling model established on one scale is applicable to another scale. This kind of scale effect is related to the linear or nonlinear degree of the downscaling model. I.e., if the model is linear, there is no scale effect, and if the model is nonlinear and the same model is

558 applied at different scale, the results will be different, and the extent of differences is related to the
559 heterogeneity of the underlying surface and the degree of nonlinearity of the model.

560 Among the five downscaling algorithms, only the DisPATCh is a linear model. There is no scale effect
561 of the model, so there will be no differences when changing the order of processing steps, i.e., no difference
562 between “averaged first and then inverted” (i.e., averaging the high-resolution downscaling predictors to
563 low-resolution and then the low-resolution SM is inverted, which corresponds to the downscaling process
564 of establishing the relationship between SM and downscaling predictors at low-resolution) and “inverted
565 first and then averaged” (i.e., inverting the high-resolution SM from the high-resolution downscaling
566 predictors and then the high-resolution SM is averaged to low-resolution, which corresponds to the
567 validating process of averaging the downscaling results to low-resolution). The pixel by pixel downscaling
568 combined with its linear model results in an unbiased downscaling method DisPATCh. Therefore, it
569 performs best among the five downscaling methods by preserving the traits of the original microwave SM
570 product as well as the smallest scale effect.

571 The other four downscaling algorithms are nonlinear, so there is a significant scale effect during the
572 model application. The models established by RF and GPR are discrete, combined with latitude and
573 longitude information, they can respond well to high and low SM conditions. However, the models
574 established by MSR and ATARK are continuous, which leads to the failure of the continuous model on
575 obtaining reliable fitting results in areas with large SM variability, resulting in large deviation in the
576 downscaling results especially around water bodies.

577 While during the interpolation process of the residuals in ATARK, as mentioned in Section 4.4, the
578 smoothing of the regression model leads to higher residuals, the residuals are still higher after interpolation.
579 These high residuals as well as the spatially smoothing effect of the interpolation process lead to the

580 "overcorrection" of the MSR bias on the other land covers around water bodies, as shown in the bias spatial
581 distribution results in Fig. 3.

582 5.2. Deterioration Effects during Downscaling

583 The results in Section 4.2 show all the five downscaling results have a decline of the accuracy than
584 RFSM with a negative G_{down} over more than 50% sites (MSR 71.6%, DisPATCh 67.6%, RF 58.1%, GPR
585 56.8% and ATARK 55.4%), which is contrary to the results of Merlin et al. (2015) and Malbéteau et al.
586 (2016). In order to investigate this phenomenon in more detail, the bar plots in Fig. 11 show the
587 performance of G_{down} and also its three components, namely G_{effi}, G_{prec}, and G_{accu}, from slope, R and
588 bias differences before and after the downscaling.

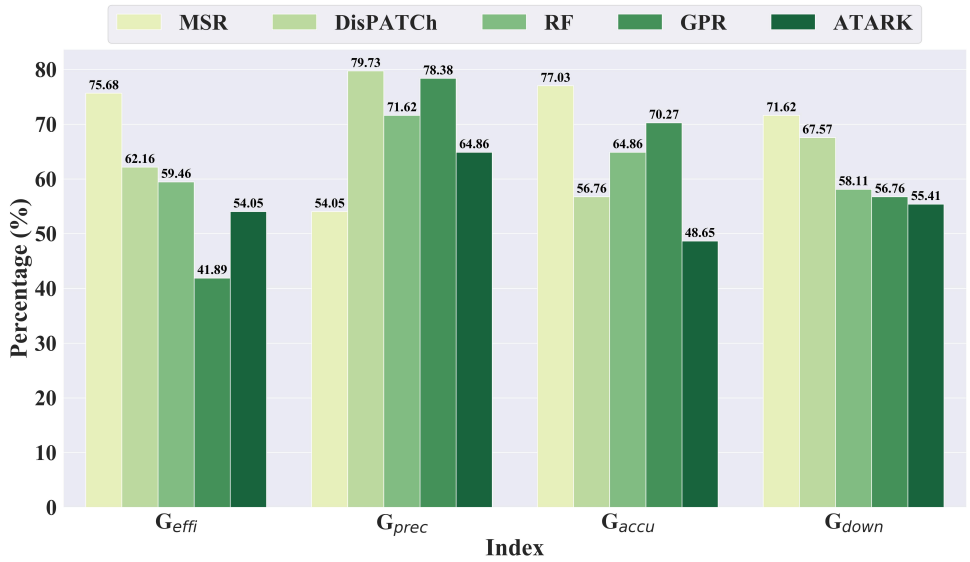

589

590 **Fig.11**. Bar plots of each downscaling method about the percentage of G_{down} and its three components
591 with negative value.

592

593 First, for G_{down}, MSR performs worst resulting from the bad performance of G_{effi} and G_{accu}, with
594 75.68% and 77.03% negative values, while it has a better G_{prec} indicating that MSR results have worse

595 slope and bias than RFSM over most sites but with a relative better R performance than other methods. For
596 DisPATCh, the 67.57% negative G_{down} may result from the bad performance of G_{prec} implying a decline
597 of R when against RFSM. The two machine learning methods, RF and GPR have similar performance in
598 G_{prec} and G_{accu} as well as G_{down} while GPR performs better in G_{effi} with less negative values
599 (41.89%). ATARK however has the best G_{down} performance caused by its good performance of the all
600 three component indices.

601 This accuracy decline phenomenon during downscaling is similar to the direct comparison results
602 against in situ data shown in Section 4. 2, where ATARK performs best, followed by DisPATCh, RF, GPR
603 and MSR considering R and bias. But there are still differences, for example MSR has the worst R value
604 (0.445) in Table 2 while it performs better in G_{prec}. Therefore, Fig. 12 was plotted to test the changes of
605 G_{effi}, G_{prec}, and G_{accu} with the different combinations of high-resolution and low-resolution statistical
606 matrix values.

607 The results indicated that these indices are suitable for single site comparison but not suitable for a
608 comprehensive comparison over several sites. Even the same G_{effi}, G_{prec}, and G_{accu} values imply
609 different magnitudes of increase or decline of the downscaling results performances as compared to
610 different original microwave product performances. Thus, the sign of these indices is more meaningful than
611 the absolute value itself when considering the validation results from different sites. Therefore the
612 mismatch of the worst R performance and the best G_{prec} performance could be explained by this different
613 potential meaning of the G_{prec} value, that is, some positive G_{prec} values may indicate a low increase of
614 the R over a site while some negative values could indicate a huge decline of the R over other sites. In total,
615 this G_{down} index is useful when comparing the downscaling results with the original microwave SM
616 product but should be used carefully when there is not a strong positive or negative trend over most sites.

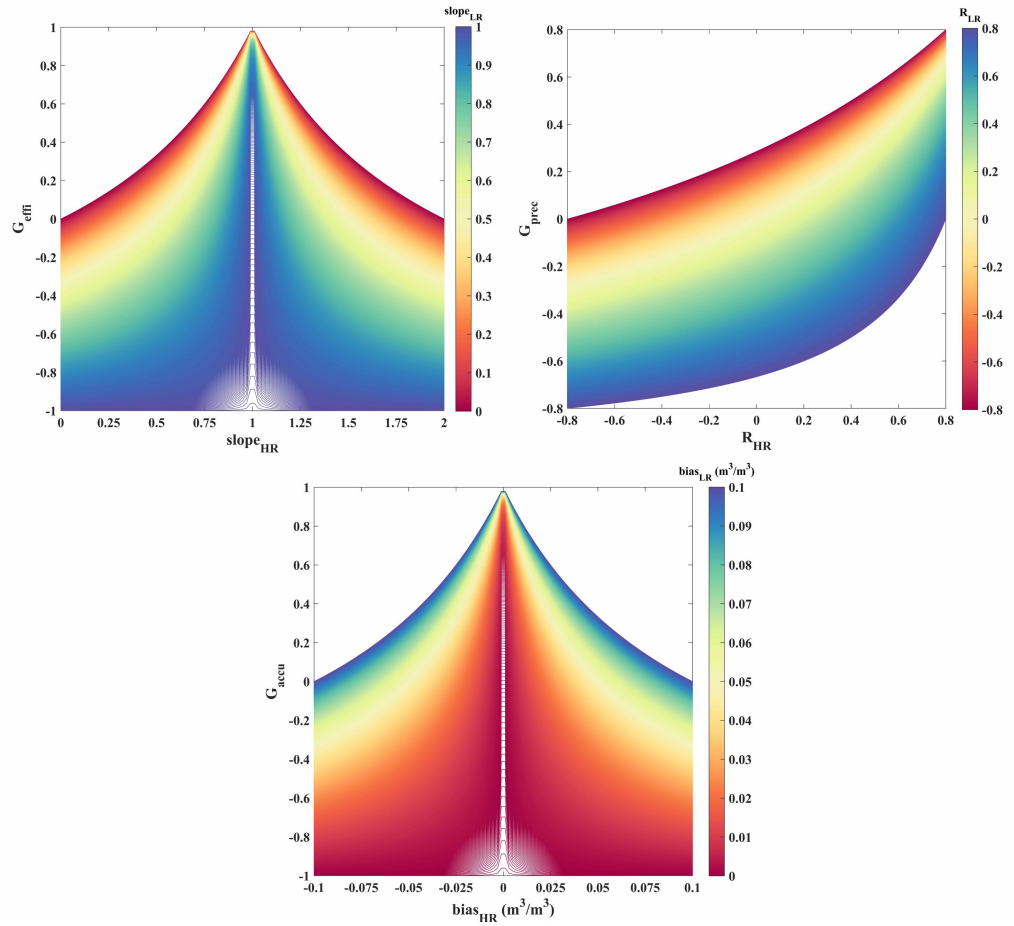

Fig.12. Changes of G_{down} and its three components with statistic results (slope, R and bias) of high-resolution downscaled soil moisture over different low-resolution RFSM conditions.

But the question is still, why there is a negative effect of the downscaling process in this study? This could result from the spatial mismatch at the fine scale resolution which is expected to be larger (Sabaghy et al., 2020; Van der Velde et al., 2012) and also the fact that original microwave products often have higher correlation with the temporally dynamic changes of the observed SM while the downscaling results have a potential to provide more spatial details and perhaps reflect more patterns about the downscaling predictors (Gruber et al., 2020; Peng et al., 2016). Although the downscaling predictors could provide more information than the original microwave SM product itself, they could also introduce errors to the downscaling process.

5.3. The Impact of Land Cover

Land cover as an important factor which can reflect and influence SM spatial distribution. It was analyzed here to further elaborate on the TCH results in Section 4.3. The variation of TCH uncertainties corresponding to land cover changes from latitude and longitude direction are shown in Fig. 13.

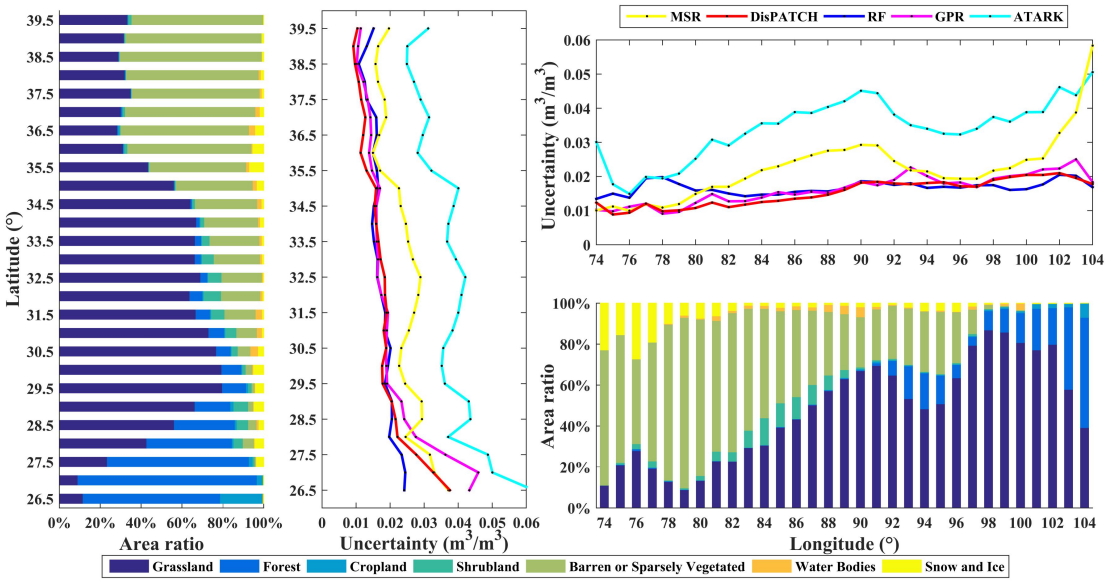

Fig.13. Changes of three-cornered hat (TCH) uncertainty with land cover on Latitude and Longitude direction.

MSR and ATARK usually have higher uncertainties than DisPATCh, RF and GPR both from latitude and longitude direction. Their uncertainties change with the percentage of vegetated land cover (the blue part in Fig. 13). While although the uncertainties of DisPATCh, RF and GPR increase too, their changes are gradual, which indicate that statistical regression based methods (MSR and ATARK) perform worse when the SM variability increases as the percentage of vegetated land cover increases. DisPATCh downscales SM in a window around the target pixel, so the performance is stable over the whole QTP except for highly vegetated areas (around 26.5° N). This results from the weaker correlation between SEE and SM there

(Malbéteau et al., 2016). Machine learning-based methods (RF and GPR) due to their model nonlinearity and flexibility can somehow capture the SM changes over high variability areas and therefore also preserve a relatively stable uncertainty.

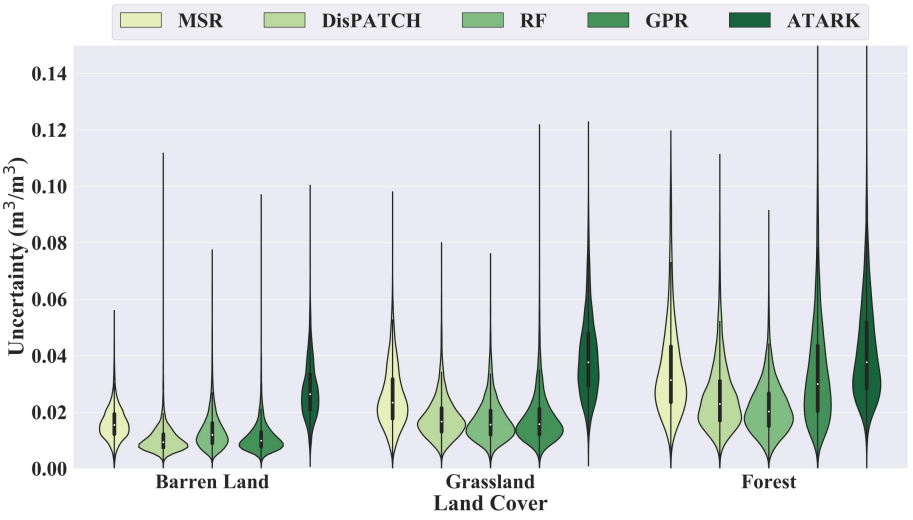

Fig.14. Violin plots (the black bar shows the third quartile, median and first quartile from top to bottom) about the three-cornered hat (TCH) uncertainty of each downscaling method over barren land, grassland and forest land cover.

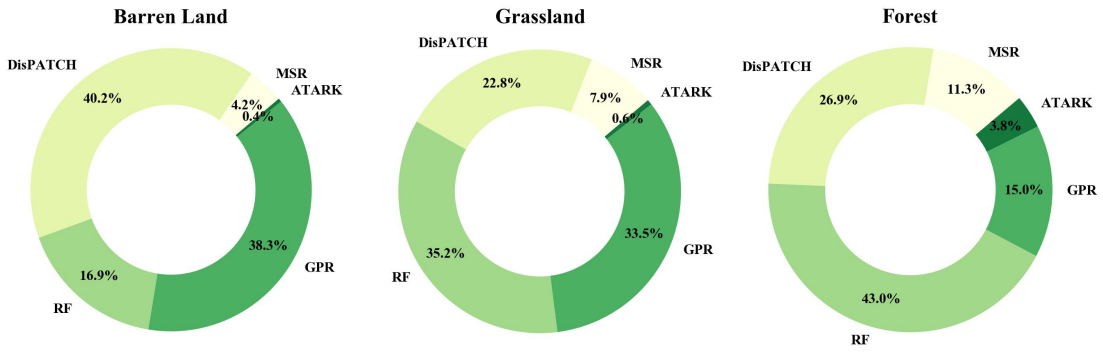

Fig.15. Circle charts about the percentage of each downscaling method with the lowest uncertainty among the five methods over barren land, grassland and forest land cover.

The violin plots and circle charts in Fig. 14 and Fig. 15 show that for barren land and sparsely vegetated land cover, DisPATCh usually has the best performance followed by GPR, RF, MSR and ATARK.

The pie graph indicates that DisPATCh has the smallest uncertainty in 40.2% of this land cover, followed by GPR, RF, MSR and ATARK (38.3%, 16.9%, 4.2%, 0.4% respectively). Under grassland, RF has the minimum uncertainties, followed by DisPATCh, GPR, MSR and ATARK. RF and GPR have the minimum uncertainty in 35.2% and 33.5% areas of grassland, followed by DisPATCh, MSR and ATARK (22.8%, 7.9%, 0.6% respectively). Under forest, RF also has the minimum uncertainty followed by DisPATCh, GPR, MSR and ATARK. RF has the minimum uncertainty in 43% area of the forest land cover, followed by DisPATCh, GPR, MSR and ATARK (26.9%, 15%, 11.3%, 3.8% respectively).

5.4. Synopsis of Validation

To perform a comprehensive comparison and to summarize the characteristics of each downscaling method, a ranked radar chart is plotted in Fig. 16. Among the five downscaling methods, DisPATCh as an unbiased method caused by its linear downscaling model and pixel-by-pixel downscaling strategy, has the best performance on preserving the spatial distribution pattern and accuracy of RFSM, followed by GPR and RF, while MSR and ATARK perform the worst resulting from the limited fitting ability of linear statistical regression model and the overcorrection phenomenon of the residual interpolation process in ATARK.

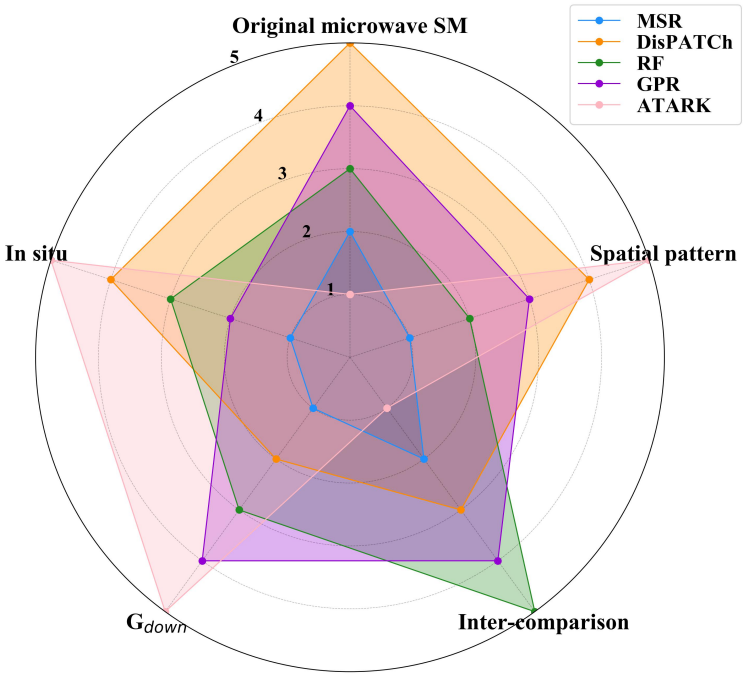

672

673 **Fig.16**. Radar chart about the ranked performance of each downscaling method when compared with
674 original microwave product, in situ measurements and according to G_{down}, inter-comparison performance
675 and spatial details. The higher the value, the better the performance.

676

677 When compared with in situ measurements, ATARK however performs best with the highest
678 correlation even better than RFSM (0.555 to 0.546), followed by RF, DisPATCh, GPR and MSR, which
679 indicates the positive effects of the residual processing strategy in ATARK and the fact that high
680 consistency with original microwave SM product to some extent could be a disadvantage for improving the
681 accuracy of the downscaling results.

682 When considering the G_{down} metric, the downscaling process has a negative effect at most sites,
683 about 71.6%, 67.6%, 58.1%, 56.8% and 55.4% for MSR, DisPATCh, RF, GPR and ATARK, respectively.
684 This negative effect of downscaling could be explained by the spatial mismatch and the trend that
685 downscaling results usually represent the spatial distribution of the downscaling predictors, not the

686 temporal changes of SM from the original microwave product. Besides, this negative effect tends to be
687 higher over heterogeneous land surface.

688 Based on inter-comparison results, RF and GPR performs better with lower uncertainty spatially and
689 RF is better than GPR over grassland and forest land cover. DisPATCh has medium uncertainty and
690 performs best over barren land or sparsely vegetated land cover as the correlation of SEE and SM is
691 stronger over arid areas. MSR and ATARK have high uncertainty spatially and ATARK performs worst
692 with high uncertainty resulted from the large deviation against other methods.

693 Considering the spatial feasibility, although showing highest SM variation spatially caused by the
694 overcorrection phenomenon of the residual interpolation process, ATARK can keep the spatial pattern of
695 RFSM well and can provide more spatial details. DisPATCh performs best with most similar spatial pattern
696 as original microwave SM product, while suffers from mosaic effects and can provide wrong SM pattern
697 over complex land surface due to that SEE alone is not sufficient to represent SM spatial patterns. GPR
698 performs better than RF both in spatial patterns and details. MSR shows smoothest spatial pattern thus
699 misses spatial details to a large degree.

700 # 6. Summary and Conclusions

701 In this study, SM downscaling was performed over QTP by five methods, namely MSR, DisPATCh,
702 RF, GPR and ATARK, to increase the spatial resolution of the original RFSM product from 0.25° to 0.01°.
703 The downscaling results were analyzed regarding four aspects, that is, comparison with the original
704 microwave SM product, comparison with in situ measurements, inter-comparison between each other, and
705 spatial feasibility analysis.

706 Due to the linear model and pixel-by-pixel downscaling strategy, DisPATCh is an unbiased

downscaling method with the highest ability of preserving the traits of microwave SM product. While to some extent, this ability could be a disadvantage for improving the accuracy of the downscaling results. Meanwhile, SEE alone is not sufficient to represent SM variations over complex land surface.

Machine learning methods, RF and GPR, perform stable in all four comparison results due to their high ability to capture nonlinear processes but provide a smoother spatial pattern. RF has lowest uncertainty over grassland and forest land cover while performs worse than GPR over barren land and sparsely vegetated land cover where DisPATCh performs best caused by the stronger correlation of SEE and SM over arid areas.

The linear regression model of MSR is not suitable for downscaling on complex land surface, resulting in the low accuracy of downscaling results and missing of spatial details, while over homogeneous land surface, its downscaling results could capture SM temporal variation well. ATARK has the highest uncertainty and large SM variation over most area of QTP caused by the overcorrection phenomenon of its residual interpolation process. However, it can also slightly improve the correlation (R) of the downscaling results and correct the bias when compared against in situ measurements as well as provide more feasible spatial patterns and details.

The availability of G_{down} in downscaling results comparison is also discussed in this study, as this index is suitable for the comparison before and after the downscaling for a single site and a single method, it is not very useful to the comprehensive comparison on several sites. Therefore, we recommended to use this index carefully and as an independent indicator from the statistic results. Based on G_{down}, accuracy decreasing is detected in all five downscaling methods, which may be caused by the spatial mismatch on fine scale and the fact that downscaling results tend to preserve spatial traits of downscaling predictors while to some extent miss the temporal changes of microwave SM product. In general, this phenomenon is

more likely to happen over complex land surface structures.

Authorship Contribution Statement

Yuquan Qu: Conceptualization, Methodology, Validation, Formal Analysis, Writing—Original Draft. Zhongli Zhu: Conceptualization, Supervision, Methodology, Formal Analysis, Funding Acquisition, Writing—Review & Editing. Carsten Montzka: Methodology, Formal Analysis, Writing—Review & Editing. Linna Chai, Shaomin Liu, Yong Ge: Methodology, Formal Analysis, Writing—Review & Editing. Jin Liu, Zheng Lu, Jie Zheng: Resources, Data Curation, Validation. Xinlei He, Tian Han: Visualization, Writing—Review & Editing.

Acknowledgements:

This study was supported by the National Natural Science Foundation of China (41671336), Strategic Priority Research Program of Chinese Academy of Sciences (XDA20100101) and State Key Laboratory of Earth Surface Processes and Resource Ecology (2017-FX-04). Meanwhile, we appreciate the Qinghai-Tibet plateau Monitoring Network, Northwest Institute of Eco-Environment and Resources, Chinese Academy of Sciences and HiWATER for providing soil moisture in situ data sets.

Declaration of competing interest:

The authors declare no conflict of interest.

References:

Ahmad, M.W., Mourshed, M., Rezgui, Y., 2017. Trees vs neurons comparison between random forest and ANN for high-resolution prediction of building energy consumption. Energy and Buildings. 147, 77-89. https://doi.org/10.1016/j.enbuild.2017.04.038

Alizadeh, M.R., Nikoo, M.R., 2018. A fusion-based methodology for meteorological drought estimation using remote sensing data. Remote Sensing of Environment. 211, 229-247. https://doi.org/10.1016/j.rse.2018.04.001

Bartalis, Z., Wagner, W., Naeimi, V., Hasenauer, S., Scipal, K., Bonekamp, H., Figa, J., Anderson, C., 2007. Initial soil moisture retrievals from the METOP-A Advanced Scatterometer (ASCAT). Geophysical Research Letters. 34. https://doi.org/10.1029/2007GL031088

Breiman, L., 2001. Random Forests. Machine Learning. 45, 5-32.

Brocca, L., Hasenauer, S., Lacava, T., Melone, F., Moramarco, T., Wagner, W., Dorigo, W., Matgen, P., Martínez-Fernández, J., Llorens, P., Latron, J., Martin, C., Bittelli, M., 2011. Soil moisture estimation through ASCAT and AMSR-E sensors: an intercomparison and validation study across Europe. Remote Sensing of Environment. 115, 3390-3408. https://doi.org/10.1016/j.rse.2011.08.003

Burapapol, K., Nagasawa, R., 2016. Mapping soil moisture as an indicator of wildfire risk using Landsat 8 images in Sri Lanna National Park, northern Thailand. Journal of Agricultural Science. 8, 107. https://doi.org/10.5539/jas.v8n10p107

Chauhan, N.S., Miller, S., Ardanuy, P., 2003. Spaceborne soil moisture estimation at high resolution: a microwave-optical/IR synergistic approach. International Journal of Remote Sensing. 24, 4599-4622. https://doi.org/10.1080/0143116031000156837

Chen, H., Zhu, Q., Peng, C., Wu, N., Wang, Y., Fang, X., Gao, Y., Zhu, D., Yang, G., Tian, J., Kang, X., Piao, S.,

767 Ouyang, H., Xiang, W., Luo, Z., Jiang, H., Song, X., Zhang, Y., Yu, G., Zhao, X., Gong, P., Yao, T., Wu, J.,
768 2013. The impacts of climate change and human activities on biogeochemical cycles on the
769 Qinghai-Tibetan Plateau. Global Change Biology. 19, 2940-2955. https://doi.org/10.1111/gcb.12277
770 Chen, S., She, D., Zhang, L., Guo, M., Liu, X., 2019. Spatial downscaling methods of soil moisture based on
771 multisource remote sensing data and its application. Water. 11, 1401. https://doi.org/10.3390/w11071401
772 Cheng, G., Wu, T., 2007. Responses of permafrost to climate change and their environmental significance,
773 Qinghai-Tibet Plateau. Journal of Geophysical Research. 112. https://doi.org/10.1029/2006JF000631
774 Crow, W.T., Wood, E.F., Dubayah, R., 2000. Potential for downscaling soil moisture maps derived from
775 spaceborne imaging radar data. Journal of Geophysical Research: Atmospheres. 105, 2203-2212.
776 https://doi.org/10.1029/1999JD901010
777 Cui, H., Jiang, L., Du, J., Zhao, S., Wang, G., Lu, Z., Wang, J., 2017. Evaluation and analysis of AMSR-2,
778 SMOS, and SMAP soil moisture products in the Genhe area of China. Journal of Geophysical Research:
779 Atmospheres. 122, 8650-8666. https://doi.org/10.1002/2017JD026800
780 Das, N.N., Entekhabi, D., Njoku, E.G., Shi, J.C., Johnson, J.T., Colliander, A., 2014. Tests of the SMAP
781 combined radar and radiometer algorithm using airborne field campaign observations and simulated data.
782 IEEE Transactions on Geoscience and Remote Sensing. 52, 2018-2028.
783 https://doi.org/10.1109/TGRS.2013.2257605
784 Ding, M., Zhang, Y., Liu, L., Zhang, W., Wang, Z., Bai, W., 2007. The relationship between NDVI and
785 precipitation on the Tibetan Plateau. Journal of Geographical Sciences. 17, 259-268.
786 https://doi.org/10.1007/s11442-007-0259-7
787 Entekhabi, D., Njoku, E.G., O'Neill, P.E., Kellogg, K.H., Crow, W.T., Edelstein, W.N., Entin, J.K., Goodman,
788 S.D., Jackson, T.J., Johnson, J., Kimball, J., Piepmeier, J.R., Koster, R.D., Martin, N., McDonald, K.C.,

789 Moghaddam, M., Moran, S., Reichle, R., Shi, J.C., Spencer, M.W., Thurman, S.W., Tsang, L., Van Zyl, J.,
790 2010. The Soil Moisture Active Passive (SMAP) mission. Proceedings of The IEEE. 98, 704-716.
791 https://doi.org/10.1109/JPROC.2010.2043918
792 Fang, B., Lakshmi, V., Bindlish, R., Jackson, T., 2018. AMSR2 soil moisture downscaling using temperature and
793 vegetation data. Remote Sensing. 10, 1575. https://doi.org/10.3390/rs10101575
794 Galindo, F.J., Palacio, J., 1999. Estimating the instabilities of N correlated clocks. In, 31st Annual Precise Time
795 and Time Interval Meeting (pp. 285-296)
796 Gruber, A., De Lannoy, G., Albergel, C., Al-Yaari, A., Brocca, L., Calvet, J.C., Colliander, A., Cosh, M., Crow,
797 W., Dorigo, W., Draper, C., Hirschi, M., Kerr, Y., Konings, A., Lahoz, W., McColl, K., Montzka, C.,
798 Muñoz-Sabater, J., Peng, J., Reichle, R., Richaume, P., Rüdiger, C., Scanlon, T., van der Schalie, R.,
799 Wigneron, J.P., Wagner, W., 2020. Validation practices for satellite soil moisture retrievals: what are (the)
800 errors? Remote Sensing of Environment. 244, 111806. https://doi.org/10.1016/j.rse.2020.111806
801 Guevara, M., Vargas, R., 2019. Downscaling satellite soil moisture using geomorphometry and machine learning.
802 PLoS One. 14, e219639. https://doi.org/10.1371/journal.pone.0219639
803 Hu, J., Wang, J., 2015. Short-term wind speed prediction using empirical wavelet transform and Gaussian
804 process regression. Energy. 93, 1456-1466. https://doi.org/10.1016/j.energy.2015.10.041
805 Im, J., Park, S., Rhee, J., Baik, J., Choi, M., 2016. Downscaling of AMSR-E soil moisture with MODIS products
806 using machine learning approaches. Environmental Earth Sciences. 75.
807 https://doi.org/10.1007/s12665-016-5917-6
808 Ines, A.V.M., Mohanty, B.P., Shin, Y., 2013. An unmixing algorithm for remotely sensed soil moisture. Water
809 Resources Research. 49, 408-425. https://doi.org/10.1029/2012WR012379
810 Jackson, T.J., Bindlish, R., Cosh, M., Gasiewski, A., Stankov, B., Klein, M., Weber, B., Zavorotny, V. 2005. Soil

moisture experiments 2004 (SMEX04) polarimetric scanning radiometer, AMSR-E and heterogeneous landscapes. In (pp. 1114-1117): IEEE

Jia, K., Liang, S., Liu, S., Li, Y., Xiao, Z., Yao, Y., Jiang, B., Zhao, X., Wang, X., Xu, S., Cui, J., 2015. Global land surface fractional vegetation cover estimation using general regression neural networks from MODIS surface reflectance. IEEE Transactions on Geoscience and Remote Sensing. 53, 4787-4796. https://doi.org/10.1109/TGRS.2015.2409563

Jin, Y., Ge, Y., Wang, J., Chen, Y., Heuvelink, G.B.M., Atkinson, P.M., 2018b. Downscaling AMSR-2 soil moisture data with geographically weighted area-to-area regression Kriging. IEEE Transactions on Geoscience and Remote Sensing. 56, 2362-2376. https://doi.org/10.1109/TGRS.2017.2778420

Jin, Y., Ge, Y., Wang, J., Heuvelink, G., Wang, L., 2018a. Geographically weighted area-to-point regression Kriging for spatial downscaling in remote sensing. Remote Sensing. 10, 579. https://doi.org/10.3390/rs10040579

Kerr, Y.H., Waldteufel, P., Wigneron, J., Delwart, S., Cabot, F., Boutin, J., Escorihuela, M., Font, J., Reul, N., Gruhier, C., Juglea, S.E., Drinkwater, M.R., Hahne, A., Martín-Neira, M., Mecklenburg, S., 2010. The SMOS mission: New tool for monitoring key elements of the global water cycle. Proceedings of the IEEE. 98, 666-687. https://doi.org/10.1109/JPROC.2010.2043032

Kim, D., Moon, H., Kim, H., Im, J., Choi, M., 2018. Intercomparison of downscaling techniques for satellite soil moisture products. Advances in Meteorology. 2018, 1-16. https://doi.org/10.1155/2018/4832423

Kim, D., Park, N., Kim, N., Kim, K., Lee, S., Kim, Y., Kim, J., Shin, D., Cho, Y., Lee, Y., 2017. Downscaling Advanced Microwave Scanning Radiometer 2 (AMSR2) soil moisture data using regression-Kriging. Journal of the Korean Cartographic Association. 17, 99-110. https://doi.org/10.16879/jkca.2017.17.2.099

Kim, J., Hogue, T.S., 2012. Improving spatial soil moisture representation through integration of AMSR-E and

MODIS products. IEEE Transactions on Geoscience and Remote Sensing . 50, 446-460. https://doi.org/10.1109/TGRS.2011.2161318

Li, J., Qu, Y., Li, C., Xie, Y., Wu, Y., Fan, J., 2015. Learning local Gaussian process regression for image super-resolution. Neurocomputing. 154, 284-295. https://doi.org/10.1016/j.neucom.2014.11.064

Li, X., Cheng, G., Liu, S., Xiao, Q., Ma, M., Jin, R., Che, T., Liu, Q., Wang, W., Qi, Y., Wen, J., Li, H., Zhu, G., Guo, J., Ran, Y., Wang, S., Zhu, Z., Zhou, J., Hu, X., Xu, Z., 2013. Heihe Watershed Allied Telemetry Experimental Research (HiWATER): scientific objectives and experimental design. Bulletin of the American Meteorological Society. 94, 1145-1160. https://doi.org/10.1175/BAMS-D-12-00154.1

Liu, J., Chai, L., Lu, Z., Liu, S., Qu, Y., Geng, D., Song, Y., Guan, Y., Guo, Z., Wang, J., Zhu, Z., 2019. Evaluation of SMAP, SMOS-IC, FY3B, JAXA, and LPRM soil moisture products over the Qinghai-Tibet Plateau and its surrounding areas. Remote Sensing. 11, 792. https://doi.org/10.3390/rs11070792

Liu, N.F., Liu, Q., Wang, L.Z., Liang, S.L., Wen, J.G., Qu, Y., Liu, S.H., 2013a. A statistics-based temporal filter algorithm to map spatiotemporally continuous shortwave albedo from MODIS data. Hydrology and Earth System Sciences. 17, 2121-2129. https://doi.org/10.5194/hess-17-2121-2013

Liu, Q., Wang, L., Qu, Y., Liu, N., Liu, S., Tang, H., Liang, S., 2013b. Preliminary evaluation of the long-term GLASS albedo product. International Journal of Digital Earth: The Recent Progress in Land Remote Sensing. 6, 69-95. https://doi.org/10.1080/17538947.2013.804601

Liu, S., Li, X., Xu, Z., Che, T., Xiao, Q., Ma, M., Liu, Q., Jin, R., Guo, J., Wang, L., Wang, W., Qi, Y., Li, H., Xu, T., Ran, Y., Hu, X., Shi, S., Zhu, Z., Tan, J., Zhang, Y., Ren, Z., 2018b. The Heihe integrated observatory network: a basin - scale land surface processes observatory in China. Vadose Zone Journal. 17, 1-21. https://doi.org/10.2136/vzj2018.04.0072

Liu, Y., Yang, Y., Jing, W., Yue, X., 2018a. Comparison of different machine learning approaches for monthly

satellite-based soil moisture downscaling over northeast China. Remote Sensing. 10, 31. https://doi.org/10.3390/rs10010031

Long, D., Bai, L., Yan, L., Zhang, C., Yang, W., Lei, H., Quan, J., Meng, X., Shi, C., 2019. Generation of spatially complete and daily continuous surface soil moisture of high spatial resolution. Remote Sensing of Environment. 233, 111364. https://doi.org/10.1016/j.rse.2019.111364

Lorenz, C., Montzka, C., Jagdhuber, T., Laux, P., Kunstmann, H., 2018. Long-term and high-resolution global time series of brightness temperature from copula-based fusion of SMAP enhanced and SMOS data. Remote Sensing. 10, 1842. https://doi.org/10.3390/rs10111842

Madadgar, S., AghaKouchak, A., Farahmand, A., Davis, S.J., 2017. Probabilistic estimates of drought impacts on agricultural production. Geophysical Research Letters. 44, 7799-7807. https://doi.org/10.1002/2017GL073606

Malbéteau, Y., Merlin, O., Molero, B., Rüdiger, C., Bacon, S., 2016. DisPATCh as a tool to evaluate coarse-scale remotely sensed soil moisture using localized in situ measurements: application to SMOS and AMSR-E data in Southeastern Australia. International Journal of Applied Earth Observation and Geoinformation. 45, 221-234. https://doi.org/10.1016/j.jag.2015.10.002

Merlin, O., Al Bitar, A., Walker, J.P., Kerr, Y., 2009. A sequential model for disaggregating near-surface soil moisture observations using multi-resolution thermal sensors. Remote Sensing of Environment. 113, 2275-2284. https://doi.org/10.1016/j.rse.2009.06.012

Merlin, O., Al Bitar, A., Walker, J.P., Kerr, Y., 2010. An improved algorithm for disaggregating microwave-derived soil moisture based on red, near-infrared and thermal-infrared data. Remote Sensing of Environment. 114, 2305-2316. https://doi.org/10.1016/j.rse.2010.05.007

Merlin, O., Escorihuela, M.J., Mayoral, M.A., Hagolle, O., Al Bitar, A., Kerr, Y., 2013. Self-calibrated

877 evaporation-based disaggregation of SMOS soil moisture: an evaluation study at 3km and 100m resolution
878 in Catalunya, Spain. Remote Sensing of Environment . 130, 25-38. https://doi.org/10.1016/j.rse.2012.11.008
879 Merlin, O., Malbéteau, Y., Notfi, Y., Bacon, S., Khabba, S., Jarlan, L., 2015. Performance metrics for soil
880 moisture downscaling methods: application to DISPATCH data in central Morocco. Remote Sensing. 7,
881 3783-3807. https://doi.org/10.3390/rs70403783
882 Merlin, O., Rudiger, C., Bitar, A.A., Richaume, P., Walker, J.P., Kerr, Y.H., 2012. Disaggregation of SMOS soil
883 moisture in southeastern Australia. IEEE Transactions on Geoscience and Remote Sensing. 50, 1556-1571.
884 https://doi.org/10.1109/TGRS.2011.2175000
885 Merlin, O., Stefan, V.G., Amazirh, A., Chanzy, A., Ceschia, E., Er-Raki, S., Gentine, P., Tallec, T., Ezzahar, J.,
886 Bircher, S., Beringer, J., Khabba, S., 2016. Modeling soil evaporation efficiency in a range of soil and
887 atmospheric conditions using a meta-analysis approach. Water Resources Research. 52, 3663-3684.
888 https://doi.org/10.1002/2015WR018233
889 Merlin, O., Walker, J., Chehbouni, A., Kerr, Y., 2008. Towards deterministic downscaling of SMOS soil moisture
890 using MODIS derived soil evaporative efficiency. Remote Sensing of Environment. 112, 3935-3946.
891 https://doi.org/10.1016/j.rse.2008.06.012
892 Mihoub, R., Chabour, N., Guermoui, M., 2016. Modeling soil temperature based on Gaussian process regression
893 in a semi-arid-climate, case study Ghardaia, Algeria. Geomechanics and Geophysics for Geo-Energy and
894 Geo-Resources. 2, 397-403. https://doi.org/10.1007/s40948-016-0033-3
895 Mohanty, B.P., Cosh, M.H., Lakshmi, V., Montzka, C., 2017. Soil moisture remote sensing: state of the science.
896 Vadose Zone Journal. 16, 1-9. https://doi.org/10.2136/vzj2016.10.0105
897 Montzka, C., Bogena, H., Zreda, M., Monerris, A., Morrison, R., Muddu, S., Vereecken, H., 2017. Validation of
898 spaceborne and modelled surface soil moisture products with cosmic-ray neutron probes. Remote Sensing.

9, 103. https://doi.org/10.3390/rs9020103

Montzka, C., Jagdhuber, T., Horn, R., Bogena, H.R., Hajnsek, I., Reigber, A., Vereecken, H., 2016. Investigation of SMAP fusion algorithms with airborne active and passive L-band microwave remote sensing. IEEE Transactions on Geoscience and Remote Sensing. 54, 3878-3889. https://doi.org/10.1109/TGRS.2016.2529659

Montzka, C., Rötzer, K., Bogena, H., Sanchez, N., Vereecken, H., 2018. A new soil moisture downscaling approach for SMAP, SMOS, and ASCAT by predicting sub-grid variability. Remote Sensing. 10, 427. https://doi.org/10.3390/rs10030427

Moran, M.S., Clarke, T.R., Inoue, Y., Vidal, A., 1994. Estimating crop water deficit using the relation between surface-air temperature and spectral vegetation index. Remote Sensing of Environment. 49, 246-263.https://doi.org/10.1016/0034-4257(94)90020-5

Narayan, U., Lakshmi, V., Jackson, T.J., 2006. High-resolution change estimation of soil moisture using L-band radiometer and radar observations made during the SMEX02 experiments. IEEE Transactions on Geoscience and Remote Sensing. 44, 1545-1554. https://doi.org/10.1109/TGRS.2006.871199

Nasta, P., Penna, D., Brocca, L., Zuecco, G., Romano, N., 2018. Downscaling near-surface soil moisture from field to plot scale: A comparative analysis under different environmental conditions. Journal of Hydrology. 557, 97-108. https://doi.org/10.1016/j.jhydrol.2017.12.017

Naz, B.S., Kollet, S., Franssen, H.H., Montzka, C., Kurtz, W., 2020. A 3 km spatially and temporally consistent European daily soil moisture reanalysis from 2000 to 2015. Scientific Data. 7. https://doi.org/10.1038/s41597-020-0450-6

Ni, J., Herzschuh, U., 2011. Simulating biome distribution on the Tibetan Plateau using a modified global vegetation model. Arctic. Antarctic. and Alpine Research. 43, 429-441.

https://doi.org/10.1657/1938-4246-43.3.429

Parinussa, R.M., Holmes, T.R.H., Wanders, N., Dorigo, W.A., de Jeu, R.A.M., 2015. A preliminary study toward consistent soil moisture from AMSR2. Journal of Hydrometeorology. 16, 932-947. https://doi.org/10.1175/JHM-D-13-0200.1

Park, S., Im, J., Park, S., Rhee, J., 2015. AMSR2 soil moisture downscaling using multisensor products through machine learning approach. In, 2015 IEEE International Geoscience and Remote Sensing Symposium (IGARSS) (pp. 1984-1987)

Pellenq, J., Kalma, J., Boulet, G., Saulnier, G.M., Wooldridge, S., Kerr, Y., Chehbouni, A., 2003. A disaggregation scheme for soil moisture based on topography and soil depth. Journal of Hydrology. 276, 112-127. https://doi.org/10.1016/S0022-1694(03)00066-0

Peng, J., Loew, A., Merlin, O., Verhoest, N.E.C., 2017. A review of spatial downscaling of satellite remotely sensed soil moisture. Reviews of Geophysics. 55, 341-366. https://doi.org/10.1002/2016RG000543

Peng, J., Loew, A., Zhang, S., Wang, J., Niesel, J., 2016. Spatial downscaling of satellite soil moisture data using a vegetation temperature condition index. IEEE Transactions on Geoscience and Remote Sensing. 54, 558-566. https://doi.org/10.1109/TGRS.2015.2462074

Peng, J., Niesel, J., Loew, A., 2015. Evaluation of soil moisture downscaling using a simple thermal-based proxy – the REMEDHUS network (Spain) example. Hydrology and Earth System Sciences. 19, 4765-4782. https://doi.org/10.5194/hess-19-4765-2015

Piles, M., Petropoulos, G.P., Sánchez, N., González-Zamora, Á., Ireland, G., 2016. Towards improved spatio-temporal resolution soil moisture retrievals from the synergy of SMOS and MSG SEVIRI spaceborne observations. Remote Sensing of Environment. 180, 403-417. https://doi.org/10.1016/j.rse.2016.02.048

Qu, Y., Liu, Q., Liang, S., Wang, L., Liu, N., Liu, S., 2014. Direct-estimation algorithm for mapping daily land-surface broadband albedo from MODIS data. IEEE Transactions on Geoscience and Remote Sensing. 52, 907-919. https://doi.org/10.1109/TGRS.2013.2245670

Qu, Y., Zhu, Z., Chai, L., Liu, S., Montzka, C., Liu, J., Yang, X., Lu, Z., Jin, R., Li, X., Guo, Z., Zheng, J., 2019. Rebuilding a microwave soil moisture product using random forest adopting AMSR-E/AMSR2 brightness temperature and SMAP over the Qinghai–Tibet Plateau, China. Remote Sensing. 11, 683. https://doi.org/10.3390/rs11060683

Ray, R., Fares, A., He, Y., Temimi, M., 2017. Evaluation and inter-comparison of satellite soil moisture products using in situ observations over Texas, U.S. Water. 9, 372. https://doi.org/10.3390/w9060372

Sabaghy, S., Walker, J.P., Renzullo, L.J., Akbar, R., Chan, S., Chaubell, J., Das, N., Dunbar, R.S., Entekhabi, D., Gevaert, A., Jackson, T.J., Loew, A., Merlin, O., Moghaddam, M., Peng, J., Peng, J., Piepmeier, J., Rüdiger, C., Stefan, V., Wu, X., Ye, N., Yueh, S., 2020. Comprehensive analysis of alternative downscaled soil moisture products. Remote Sensing of Environment. 239, 111586. https://doi.org/10.1016/j.rse.2019.111586

Sabaghy, S., Walker, J.P., Renzullo, L.J., Jackson, T.J., 2018. Spatially enhanced passive microwave derived soil moisture: capabilities and opportunities. Remote Sensing of Environment. 209, 551-580. https://doi.org/10.1016/j.rse.2018.02.065

Sahoo, A.K., De Lannoy, G.J.M., Reichle, R.H., Houser, P.R., 2013. Assimilation and downscaling of satellite observed soil moisture over the Little River Experimental Watershed in Georgia, USA. Advances in Water Resources. 52, 19-33. https://doi.org/10.1016/j.advwatres.2012.08.007

Sánchez-Ruiz, S., Piles, M., Sánchez, N., Martínez-Fernández, J., Vall-llossera, M., Camps, A., 2014. Combining SMOS with visible and near/shortwave/thermal infrared satellite data for high resolution soil moisture estimates. Journal of Hydrology. 516, 273-283. https://doi.org/10.1016/j.jhydrol.2013.12.047

965 Schaefer, A.J., Magi, B.I., 2019. Land-cover dependent relationships between fire and soil moisture. Fire. 2, 55.
966 https://doi.org/10.3390/fire2040055
967 Song, P., Huang, J., Mansaray, L.R., 2019. An improved surface soil moisture downscaling approach over cloudy
968 areas based on geographically weighted regression. Agricultural and Forest Meteorology. 275, 146-158.
969 https://doi.org/10.1016/j.agrformet.2019.05.022
970 Srivastava, P.K., Han, D., Ramirez, M.R., Islam, T., 2013. Machine learning techniques for downscaling SMOS
971 satellite soil moisture using MODIS land surface temperature for hydrological application. Water Resources
972 Management. 27, 3127-3144. https://doi.org/10.1007/s11269-013-0337-9
973 Su, Z., Wen, J., Dente, L., van der Velde, R., Wang, L., Ma, Y., Yang, K., Hu, Z., 2011. The Tibetan Plateau
974 observatory of plateau scale soil moisture and soil temperature (Tibet-Obs) for quantifying uncertainties in
975 coarse resolution satellite and model products. Hydrology and Earth System Sciences. 15, 2303-2316.
976 https://doi.org/10.5194/hess-15-2303-2011
977 Tavella, P., Premoli, A., 1994. Estimating the instabilities of N clocks by measuring differences of their readings.
978 Metrologia. 30, 479. https://doi.org/10.1088/0026-1394/30/5/003
979 Van der Velde, R., Salama, M.S., van Helvoirt, M.D., Su, Z., Ma, Y., 2012. Decomposition of uncertainties
980 between coarse MM5–Noah-Simulated and fine ASAR-retrieved soil moisture over central Tibet. Journal of
981 Hydrometeorology. 13, 1925-1938. https://doi.org/10.1175/JHM-D-11-0133.1
982 Wanders, N., Karssenberg, D., de Roo, A., de Jong, S.M., Bierkens, M.F.P., 2014. The suitability of remotely
983 sensed soil moisture for improving operational flood forecasting. Hydrology and Earth System Sciences. 18,
984 2343-2357. https://doi.org/10.5194/hess-18-2343-2014
985 Wang, J., Ling, Z., Wang, Y., Zeng, H., 2016. Improving spatial representation of soil moisture by integration of
986 microwave observations and the temperature–vegetation–drought index derived from MODIS products.

ISPRS Journal of Photogrammetry and Remote Sensing. 113, 144-154. https://doi.org/10.1016/j.isprsjprs.2016.01.009

Wu, J., Gao, X.J., 2013. A gridded daily observation dataset over China region and comparison with the other datasets (in Chinese). Chinese Journal of Geophysics. 56, 1102-1111.

Wu, W., Dickinson, R.E., 2004. Time scales of layered soil moisture memory in the context of land–atmosphere interaction. Journal of Climate. 17, 2752-2764. https://doi.org/10.1175/1520-0442(2004)017<2752:TSOLSM>2.0.CO;2

Wu, X., Walker, J.P., Rudiger, C., Panciera, R., Gao, Y., 2017. Intercomparison of alternate soil moisture downscaling algorithms using active–passive microwave observations. IEEE Geoscience and Remote Sensing Letters. 14, 179-183. https://doi.org/10.1109/LGRS.2016.2633521

Xiao, Z., Liang, S., Wang, J., Chen, P., Yin, X., Zhang, L., Song, J., 2014. Use of general regression neural networks for generating the GLASS leaf area index product from time-series MODIS surface reflectance. IEEE Transactions on Geoscience and Remote Sensing. 52, 209-223. https://doi.org/10.1109/TGRS.2013.2237780

Xiao, Z., Liang, S., Wang, J., Xiang, Y., Zhao, X., Song, J., 2016. Long-time-series global land surface satellite leaf area index product derived from MODIS and AVHRR surface reflectance. IEEE Transactions on Geoscience and Remote Sensing. 54, 5301-5318. https://doi.org/10.1109/TGRS.2016.2560522

Yang, K., 2013. A multi-scale soil moisture and freeze-thaw monitoring network on the Third Pole. Bulletin of the American Meteorological Society. 94, 1907-1916. https://doi.org/10.1175/bams-d-12-00203.1

Yang, K., Ye, B., Zhou, D., Wu, B., Foken, T., Qin, J., Zhou, Z., 2011. Response of hydrological cycle to recent climate changes in the Tibetan Plateau. Climatic Change. 109, 517-534. https://doi.org/10.1007/s10584-011-0099-4

Yu, G., Di, L., Yang, W., 2008. Downscaling of global soil moisture using auxiliary Data. In, IEEE International Geoscience Remote Sensing Symposium (pp. 230-233)

Zeng, J., Chen, K., Bi, H., Chen, Q., 2016. A preliminary evaluation of the SMAP radiometer soil moisture product over United States and Europe using ground-based measurements. IEEE Transactions on Geoscience and Remote Sensing. 54, 4929-4940. https://doi.org/10.1109/TGRS.2016.2553085

Zhan, X., Houser, P.R., Walker, J.P., Crow, W.T., 2006. A method for retrieving high-resolution surface soil moisture from hydros L-band radiometer and radar observations. IEEE Transactions on Geoscience and Remote Sensing. 44, 1534-1544. https://doi.org/10.1109/TGRS.2005.863319

Zhang, X., Zhou, J., Gottsche, F., Zhan, W., Liu, S., Cao, R., 2019. A method based on temporal component decomposition for estimating 1-km all-weather land surface temperature by merging satellite thermal infrared and passive microwave observations. IEEE Transactions on Geoscience and Remote Sensing. 57, 4670-4691. https://doi.org/10.1109/TGRS.2019.2892417

Zhang, Y., Ohata, T., Kadota, T., 2003. Land-surface hydrological processes in the permafrost region of the eastern Tibetan Plateau. Journal of Hydrology. 283, 41-56. https://doi.org/10.1016/S0022-1694(03)00240-3

Zhao, L., Yang, K., Qin, J., Chen, Y., Tang, W., Montzka, C., Wu, H., Lin, C., Han, M., Vereecken, H., 2013. Spatiotemporal analysis of soil moisture observations within a Tibetan mesoscale area and its implication to regional soil moisture measurements. Journal of Hydrology. 482, 92-104. https://doi.org/10.1016/j.jhydrol.2012.12.033

Zhao, W., Sánchez, N., Lu, H., Li, A., 2018. A spatial downscaling approach for the SMAP passive surface soil moisture product using random forest regression. Journal of Hydrology. 563, 1009-1024. https://doi.org/10.1016/j.jhydrol.2018.06.081